International Journal of Hydrogen Energy 237 (2026) 155320

Contents lists available at ScienceDirect

International Journal of Hydrogen Energy

journal homepage: www.elsevier.com/locate/he

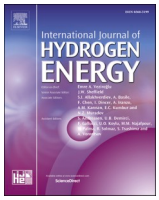

Micro-kinetics of dibenzyltoluene liquid organic hydrogen carrier reactions over alumina-supported nickel catalyst

Emilija Rakić Krstić [a,b], Filip Bergelj [a], Anže Prašnikar [a], Brett Pomeroy [a], Blaž Likozar [a,*]

[a] Department of Catalysis and Chemical Reaction Engineering, National Institute of Chemistry, 1000 Ljubljana, Slovenia
[b] Faculty of Chemistry and Chemical Engineering, University of Maribor, 2000 Maribor, Slovenia

ARTICLE INFO

Keywords:
Dibenzyl toluene
Liquid organic hydrogen carriers (LOHCs)
Hydrogenation
Reaction
Micro-kinetics
Model

ABSTRACT

As the global shift towards green energy accelerates to reduce CO_2 emissions and address the greenhouse effect, this study highlights the crucial role of hydrogen storage and transportation. This research investigates the hydrogenation of dibenzyl toluene (DBT), a liquid organic hydrogen carrier, alongside a solution containing dibenzyltoluene (DBB) and dibenzylethylbenzene (DBEB), utilizing cost-effective 5 wt% Ni/Al_2O_3 catalyst. Laboratory-synthesized catalysts with 5-10 wt% Ni/Al_2O_3 were evaluated and compared against commercial catalysts where much higher performance was achieved using our catalyst. The impact of various experimental parameters, including temperature, pressure, catalyst mass, and initial LOHC concentration, was thoroughly explored (>1600 exp. points). A micro-kinetic model was developed for a commercially available 5 wt% Ni/Al_2O_3 catalyst, and recycling tests were performed to assess the catalyst's activity and longevity. The results indicate that the activation energies for the hydrogenation of DBT range from 60 to 79 kJ/mol, with the first step demonstrating the highest activation energy. Furthermore, kinetic parameters for the remaining components in the reaction mixture were defined. The model encompasses all reaction conditions, incorporating the number of metallic sites representing the catalyst's active sites, thereby providing a description of the experimental results and facilitating advancements in catalyst synthesis and the potential for LOHC utilisation.

1. Introduction

In today's context, environmental consciousness is increasingly pivotal. Acknowledging the finite nature of certain Earth resources, the search for alternatives becomes imperative [1]. Notably, fossil fuels stand out, not just due to their limited availability, but also their significant carbon footprint, particularly in combustion applications like vehicles and stationary power generation [2]. Hydrogen emerges as a clean fuel option, reacting with oxygen in fuel cells to produce only water as a byproduct, thereby mitigating not just carbon dioxide emissions but also other harmful substances [3]. Abundant in water, hydrogen offers a versatile solution for balancing fluctuating energy sources such as hydro and wind power, allowing surplus electrical energy to be harnessed for water electrolysis to produce hydrogen, which can be converted back to electrical energy during shortages [4]. Hydrogen exhibits the highest gravimetric energy density compared to conventional fuels like gasoline and diesel, with values around 120 kJ/g, making it significantly more efficient by mass [5]. However, its extremely low density poses storage challenges, necessitating advanced storage methods [6]. High-pressure storage and liquid hydrogen storage are conventional approaches, each with its own technological and safety considerations [7]. Metal hydrides offer a promising avenue for hydrogen storage, leveraging chemisorption and physisorption mechanisms, although practical challenges include reversibility, material stability, safety and kinetics [8]. Another emerging method, central to this research, involves liquid organic hydrogen carriers (LOHCs), which offer storage capacities of up to 6-7 wt%, providing a potentially efficient and reversible means of hydrogen storage [9]. These compounds exist in both saturated and unsaturated forms, featuring double or triple bonds. In the presence of hydrogen, unsaturated compounds undergo hydrogenation, resulting in saturated forms [1]. Conversely, dehydrogenation facilitates the retrieval of hydrogen, regenerating the unsaturated compound alongside hydrogen. This mode of hydrogen storage within organic molecules facilitates easier transport and storage without requiring high pressures, low temperatures, or storage losses [5]. Many compounds utilized as LOHCs exhibit physical properties similar to gasoline or diesel, enabling their storage using existing infrastructure, thus facilitating the potential integration of this technology into

* Corresponding author. Department of Catalysis and Chemical Reaction Engineering, National Institute of Chemistry, Hajdrihova, 1001, Ljubljana, Slovenia.
E-mail address: blaz.likozar@ki.si (B. Likozar).

https://doi.org/10.1016/j.ijhydene.2026.155320
Received 24 February 2026; Received in revised form 17 April 2026; Accepted 28 April 2026
Available online 3 May 2026

mainstream use if sufficiently developed for commercial application [10].

Despite the extensive research devoted to dibenzyltoluene-based liquid organic hydrogen carrier (LOHC) systems, most existing studies primarily focus on catalyst screening and overall conversion performance, with a strong emphasis on noble metal catalysts such as Ru, Pd, and Pt [11–13]. Kinetic descriptions are typically based on lumped or intrinsic rate expressions that are valid only under narrowly defined conditions, offering limited insight into the underlying surface phenomena and catalyst structure–activity relationships [14]. Furthermore, industrial dibenzyltoluene is inherently a multicomponent mixture containing dibenzylbenzene and dibenzylethylbenzene, yet this complexity is often neglected in kinetic modelling. As a result, the connection between catalyst surface properties, reaction kinetics, and reactor-scale performance remains insufficiently understood, particularly for nickel-based catalysts despite their clear economic and industrial relevance.

In this work, these limitations are addressed through a comprehensive reaction engineering and microkinetic investigation of the hydrogenation of industrial dibenzyltoluene mixtures over alumina-supported nickel catalysts. Both a commercial 5 wt% Ni/Al_2O_3 catalyst and synthesized catalysts with nickel loadings between 5 and 10 wt% are studied, with particular focus on metallic nickel sites as the active centres for DBT hydrogenation. A Langmuir–Hinshelwood-based microkinetic model is developed, explicitly incorporating adsorption, surface reaction, and site balance equations, with independently measured nickel surface site densities introduced as physically meaningful parameters. Validated over a wide range of operating conditions, this integrated approach provides deeper mechanistic understanding of nickel-catalysed LOHC hydrogenation and enables a more detailed and predictive description of Ni/Al_2O_3 catalyst performance than has been previously reported.

2. Literature review

Dibenzyl toluene (DBT) is one of the well-established and researched compounds suitable for use as a LOHC. Due to physicochemical properties it is commonly utilized in the industry as a heat transfer oil. The hydrogenated form of DBT is known as perhydro-dibenzyl toluene (perhydro-DBT) [15]. Table 1 presents key physical and chemical attributes of both DBT and perhydro-DBT compounds. The temperature range at which both compounds are in the liquid state is quite broad, ensuring flexible operation. Moreover, their high ignition temperature reduces the risk associated with their use. A low vapor pressure is advantageous as it leads to minimal losses, yielding hydrogen of higher purity. However, one challenge with DBT lies in its elevated viscosity, which complicates pumping and mass transport during reactions. Consequently, supplementary solvents are often used with DBT to reduce viscosity [2,16–18].

The hydrogen storage capacity for DBT is 6.2 wt% or 56.4 kg/m^3, (which is equivalent to 70 bar of compressed H_2 at 0 °C) with an energy density of 1.9 kWh/L. However, considering limitations in dehydrogenation, these values decrease to 6 wt% and 1.8 kWh/L [19]. Compared to N-ethylcarbazole, another compound established as an LOHC, the physical properties of DBT are much closer to conventional diesel, facilitating easier integration into existing infrastructure.

Table 1
Physical and chemical properties of DBT and Perhydro-DBT compounds[2, 16–18].

	Dibenzyl toluene	Perhydro-dibenzyl toluene
Density, kg/L	1.04	0.91
Temperature range of liquid phase, °C	−39 – 390	−45 – 354
Flash point (Ignition temperature), °C	207 (450)	183
Dynamic viscosity at 20 °C, mPas	44.1	258
Vapor pressure at 40 °C, Pa	0.07	0.04

Recent literature shows a clear predominance of noble metal catalysts, especially Pt, Ru, Rh, and Pd, supported mainly on alumina-based materials [13,20–27]. According to comparative studies, Rh/Al_2O_3 exhibits the highest hydrogenation activity, while Pt/Al_2O_3 systems generally show superior performance in dehydrogenation [20]. These findings confirm that noble metals define the current performance benchmark, although their high cost remains a key limitation for industrial application.

Among noble metals, platinum-based catalysts have been studied most extensively, particularly regarding structure–activity relationships. Pt/Al_2O_3 catalysts show strong sensitivity to Pt loading [23], nanoparticle size [28], and promoter addition [21,22,26]. Increasing Pt loading improves dehydrogenation performance, with 5 wt% Pt/Al_2O_3 outperforming lower loadings [23]. At the same time, nanoparticle size influences both activity and selectivity, with smaller particles promoting higher activity but also increasing formation of undesired by-products [28]. Promoter effects further enhance catalytic performance: CrOx improves reversible hydrogenation–dehydrogenation [21], Mo_2C reduces apparent activation energy and improves stability [22], while NbO_x modifies surface hydrogen interactions and active site availability [26]. These results demonstrate that Pt performance is strongly governed by metal–support and metal–promoter interactions.

Ruthenium-based catalysts represent another important class of highly active materials [13,24,29–31]. Ru/Al_2O_3 has been widely used for both kinetic modelling and mechanistic studies [13,29], while alternative supports such as MgO [24] and ZrO_2 [31] have demonstrated that support properties critically influence catalytic behaviour. In particular, Ru/MgO exhibits enhanced activity due to the presence of both homolytic and heterolytic hydrogen activation sites at the metal–support interface [24], whereas Al_2O_3-supported systems typically allow only homolytic dissociation. Similarly, Ru/ZrO_2 shows strong dependence on surface hydroxylation and structural properties [31]. These findings highlight the decisive role of support chemistry in determining catalytic activity.

Palladium catalysts have also been investigated, particularly in the context of hydrogenation using multicomponent gas mixtures [32]. Pd/Al_2O_3 systems demonstrated high selectivity and efficiency in hydrogen uptake from CO- and CO_2-containing streams [32], suggesting potential for flexible hydrogen integration. However, comparative studies indicate that Pd generally exhibits lower hydrogenation activity than Rh and Ru under standard conditions [20].

Nickel-based catalysts have gained increasing attention as cost-effective alternatives to noble metals [12,14,33–35]. Although Ni catalysts typically show lower intrinsic activity, their performance can be significantly enhanced through support engineering. Mesoporous SiO_2–Al_2O_3 supports improve Ni catalytic behaviour by combining Lewis and Brønsted acidity, facilitating aromatic adsorption and hydrogen activation via spillover mechanisms [34]. Under optimised conditions, Ni/Al_2O_3–SiO_2 catalysts have demonstrated rapid hydrogenation rates comparable to noble metals [33]. Intrinsic kinetic studies further provided detailed activation energies and reaction orders for DBT and BT hydrogenation over Ni catalysts [14,35], confirming their relevance for large-scale applications.

From a mechanistic perspective, DBT hydrogenation proceeds via a sequential pathway involving partially hydrogenated intermediates (Fig. 1) [13,14,29]. The most widely accepted mechanism follows a side–side–middle sequence, in which the outer aromatic rings are hydrogenated first, forming H6-DBT and H12-DBT intermediates prior to full hydrogenation to H18-DBT [29]. Accumulation of H12-DBT and higher activation energy for the final hydrogenation step confirm that the last stage is rate-determining [13,14]. Similar stepwise pathways have been reported for benzyltoluene systems, involving H6-BT as an intermediate [35].

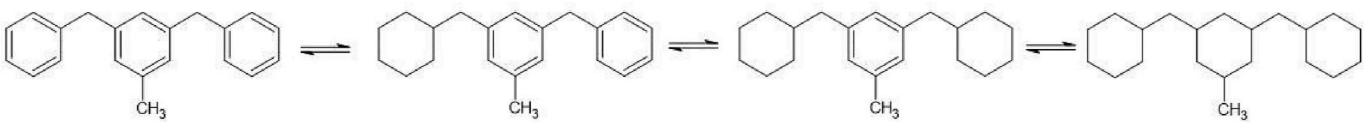

Fig. 1. DBT Hydrogenation reaction scheme.

Kinetic modelling of DBT/MBT systems has evolved from simple empirical models to more advanced mechanistic descriptions. Power-law approaches provide simplified rate expressions, while Langmuir–Hinshelwood models incorporate adsorption and surface reactions and show good agreement with experimental data at high hydrogenation degrees and elevated pressures [13]. More recently, microkinetic models have been developed to account for detailed reaction networks and hydrogen solubility effects over Ru/Al_2O_3 catalyst [36]. Intrinsic kinetic studies over Ni catalysts further quantified reaction orders and activation energies for individual steps [14,35], demonstrating the necessity of multistep modelling approaches.

Reported activation energies vary depending on catalyst and reaction step. For Ni/Al_2O_3, activation energies for DBT hydrogenation steps range from approximately 56 to 65 kJ/mol, with the final hydrogenation step identified as rate-determining [14]. Noble metal systems show broader ranges, including approximately 67 kJ/mol for hydrogenation and 83 kJ/mol for dehydrogenation in comparative studies [20], while Ru-based systems may exhibit lower apparent activation energies depending on measurement method [37].

Comparative studies position DBT/MBT against other LOHCs. DBT offers higher hydrogen capacity and superior thermal stability than N-ethylcarbazole (NEC) and toluene-based systems, with lower impurity formation during cycling and no issues of melting point or volatility at operating temperatures [18,36]. For example, hydrogenation tests at similar conditions showed higher hydrogen capacity for DBT (about 4 wt % under given conditions) than 9-ethylcarbazole (2.79 wt%) [36]. NEC has been extensively mechanistically studied and exhibits high activity on Ru catalysts, but suffers from high melting point and lower thermal stability [13].Toluene and methylcyclohexane systems benefit from low cost and existing process knowledge but face challenges from toxicity, flammability, higher vapor pressures and more pronounced side reactions (disproportionation, dealkylation) during dehydrogenation [38].Recent reviews conclude that DBT is currently among the most promising LOHCs for stationary storage and transport, while NEC remains attractive for mobility where lower dehydrogenation temperatures are prioritised [39].

In this context, Hydrogenious LOHC Technologies GmbH has played a pioneering role in advancing hydrogen storage concepts based on reversible hydrogenation–dehydrogenation cycles of hydrogen-lean/hydrogen-rich pairs such as benzyltoluene (BT/H12-BT) and dibenzyltoluene (DBT/H18-DBT) [7,39,40].

Among these, the DBT/H18-DBT system has emerged as one of the most technologically mature LOHC candidates due to its excellent thermal stability, favourable safety characteristics, and strong techno-economic performance in large-scale applications [19,41]. However, its practical deployment is still limited by relatively high dehydrogenation temperatures and diffusion-related constraints, which motivate the development of improved carrier systems and catalyst formulations [19,40].

Consequently, alternative and mixed LOHC systems based on BT and DBT have attracted increasing research interest. In particular, BT/DBT mixtures have been shown to exhibit improved transport properties, including reduced viscosity at lower temperatures and enhanced hydrogen release rates, with reported increases of up to 12–16% compared to pure DBT systems [39]. These findings, together with recent reviews highlighting benzyltoluene-based carriers as key candidates alongside DBT and other homocyclic systems, confirm the growing importance of BT–DBT platforms as complementary and industrially relevant LOHC systems [40,42].

3. Methodology and analysis

3.1. Materials

All reactants and gases were purchased from various suppliers and used without further treatment: hexane (>99%, Supelco), dibenzyl toluene (>99%, Biosynth), dodecane (>99%, TCI), nitrogen (5.0, Messer), hydrogen (5.0, Messer). The catalyst used was nickel on γ-alumina with a 5 wt% nickel content in pellet form (>98%, Riogen). For the preparation of the custom catalyst, nickel (II) nitrate (>97%, Sigma Aldrich) and γ-alumina (Spheralite 537, Procatalyse).

3.2. Preparation of the catalyst

A catalyst with 5 wt% nickel was prepared for comparison with commercially prepared one (Riogen, Ni/Al2O3), followed by versions with 7 wt% and 10 wt wt.% nickel on alumina. For catalyst preparation, the incipient wetness impregnation (IWI) method was employed. Pellets of pure γ-alumina were initially ball-milled and sieved through a 100 μm mesh. An impregnation solution was then prepared by dissolving nickel nitrate in water. The IWI method differs from other impregnation methods in that it does not involve excess impregnation solution; rather, the volume added to the catalyst equals the volume of open pores. The solution, containing dissolved active substance, penetrates all pores and, upon drying, results in uniformly distributed active substance within the catalyst pores. The volume of pores in the alumina had already been predetermined. Thus, the correct amount of nickel for the given catalyst was dissolved in this volume of water, slowly added to the alumina, and stirred with a pestle until a homogeneous mixture was obtained. After overnight drying to evaporate all water, the mixture was further calcined in a tube furnace for 3 h at 400 °C to remove any remaining substances and leave only the oxidized form of nickel in the pores. This oxidized form was ground into the powder before the reduction, as it could agglomerate during drying and calcination. Before the catalytic tests, the samples were reduced as decribed in the following text to form metallic Ni.

3.3. Reaction setup

Experimental data for kinetic modeling were obtained using a batch reactor system, Parr 5000. This system allows for the simultaneous execution of up to six parallel reactions in individual batch reactors with a 75 mL volume. Controlled by a computer, the system enables continuous monitoring of temperature, pressure, and other reaction parameters in real time for each reaction. Uniform stirring is maintained across all reactors using magnetic stirrers. Given the hydrogenation nature of the reaction, hydrogen is introduced into the reactor at high pressure, while the liquid volume is approximately 40 mL. Typically, the ratio of DBT to hexane is 1:3, although variations of 1:7 and 3:5 were also explored. Additionally, 1 mL of dodecane is added to each reaction to serve as a reference peak in gas chromatography-mass spectrometry (GC-MS) analysis. For each aromatic ring in DBT, 3 mol of hydrogen are required for complete hydrogenation, totaling 9 mol for the entire molecule. Sampling during the reaction is facilitated through a dedicated line, equipped with a filter to prevent solid particles from contaminating the sample vial. PET 0.2 μm filters are employed for this

purpose. Before each sampling, the volume of three samples is purged from the line to ensure the integrity of the sample. Sample is collected before the reactor sealing, continuing upon reaching the desired reaction temperature, and subsequently at predetermined intervals.

To ensure the absence of intraparticle mass transfer limitations, a small catalyst particle size is needed. Therefore, the catalyst pellets were ground using a ball mill at a frequency of 30 Hz for 15 min. Following grinding, the catalyst was sieved using a 100 μm mesh, resulting in particle sizes smaller than 100 μm.

Nickel catalyst is inherently oxidized and inert (on the surface in the form of NiO) under standard conditions, requiring pre-reduction before its utilisation in the reaction. To effectuate this, 100 mg aliquots of the catalyst were introduced into a tubular furnace. The furnace underwent an initial purge with nitrogen for approximately 15 min to expel residual air. Subsequently, a hydrogen flow of 150 mL/min was introduced, while the temperature program of the furnace was set to a 3-h duration at 400 °C (as NiO is typically reduced at this temperature to form Ni), with a heating rate of five degrees per minute. On the subsequent day, all components for the reaction were prepared, culminating in the addition of the catalyst as the final component. Promptly thereafter, the reactor was swiftly sealed and purged with nitrogen to minimize catalyst exposure to atmospheric air and prevent oxidation. Following this, a hydrogen purge was conducted within the reactor, with pressure monitoring until stabilization, thereby enabling leak detection. Upon achieving the desired pressure, the temperature program was initiated.

3.4. Analytical method

The composition of the samples was determined through GC-MS analysis. To ensure an appropriate concentration range for GC-MS analysis, the samples underwent dilution. Specifically, each vial was filled with 1 mL of hexane and 0.15 mL of the sample, with meticulous recording of corresponding masses.

The GC-MS (2010 Ultra, Shimadzu, Kyoto, Japan) setup, incorporated an automated sampler, facilitating the loading of vials into the rack and the initiation of the designated protocol. Employing the Zebron ZB-5MSi-MS capillary column (60 m × 0.25 mm x 0.25 μm), the system underwent two hexane flushes before sample introduction to eliminate residual contaminants. Needle cleaning was also performed using hexane. The column temperature profile began at 100 °C for 3 min, followed by a ramp to 277 °C at a rate of 25 °C/min, maintaining this temperature for 6 min. Subsequently, a further ramp to 330 °C at 15° per minute ensued, with this temperature sustained for an additional five and a half minutes. Each sample analysis had a duration of approximately 25 min, mass spectrometry was utilized to ascertain reactant concentrations. Regarding dodecane, the absolute concentration in the sample held little significance; solely the peak area was utilized for the normalization of all samples.

3.4.1. Introducing the correlation factor

For DBT actual concentrations were required, prompting the acquisition of peak area conversion factors. Upon chromatogram analysis, it became evident that at the onset of the reaction, not only DBT but also similar compounds were present in reactant mixture: dibenzyl benzene (DBB), dibenzyl ethyl benzene (DBEB). Given their structurally similar nature, differing only in the presence of methyl or ethyl groups, it was assumed that hydrogenation proceeded similarly for all these compounds. Therefore, kinetic data were determined for all compounds except dibenzyl ethyl benzene with a methyl group on the side ring, which was present in negligible quantities. Thus, there were three initial compounds in the reactor, each capable of undergoing three hydrogenation steps, resulting in a total of 12 potential compounds.

Typically, calibration curves using standards would be prepared to obtain conversion factors. However, standards for DBB, DBT, and DBEB were unavailable, prompting the exploration of an alternative approach. Since the reactor contained a known volume of liquid reactant, the initial concentration could be calculated accordingly. Using the ratios of peak areas for DBB, DBT, and DBEB, their proportions in the initial solution could also be determined. Due to the high thermal stability of the reactants (no decomposition into by-products), it was assumed that the total concentration of reactants and all hydrogenated forms remained constant throughout the reaction, as carbon compounds react in a 1:1 M ratio in all reactions. This condition is also known as carbon balance. This parameter served as a measure of successful reaction completion if it remained within the range of 0.8 to 1.1 for all reactions.

Analysis via GC-MS revealed that the initial mixture contained, in addition to DBT, other compounds, namely DBB and DBEB. Given that these compounds possess different groups attached to the aromatic ring, the presence of multiple isomers is possible. This could not be determined by GC-MS, as all isomers would have the same molar mass; however, it is assumed that the influence of this on reaction kinetics is negligible. The mixture contained 66.9% DBT, 16.5% DBB, and 16.5% DBEB.

3.5. Catalyst characterisation

X-ray diffraction (XRD) patterns were characterized using PW3040/60 X'Pert PRO MPD diffractometer at 35 kV and 45 mA with Cu Kα radiation source ($\lambda = 0.154056$ nm) in the 2θ range from 10° to 80°, and using JCPDS database for reference. Surface and textural properties of the commercial catalyst were analyzed with nitrogen physisorption; specifically, adsorption-desorption isotherms to determine the specific surface area (S_{BET}), average pore diameter (d_p), and pore volume (V_P) using an ASAP 2020 gas adsorption instrument (Micrometrics, Norcross, GA, USA). Energy dispersive spectroscopy (EDS) was performed using a Carl Zeiss SUPRA35 VP scanning electron microscope (SEM), fitted with an Inca 400 EDS detector from Oxford Instruments. Mapping was performed with a 20 kV electron beam and a 120 μm aperture size.

The Ni dispersion was measured using O_2 PSO (pulsed surface oxidation). The analyses were performed on Belcat II (Microtrac Retsch) coupled to mass spectrometer Belmass II Microtrac Retsch. Firstly around 100 mg of the catalyst was heated to 500 °C in 10% O2/He. Afterwards, the temperature decreased to 40 °C, and 5% H_2/Ar was introduced. We increased the temperature with the heating rate of 10 °C/min to 500 °C and held the temperature for 20 min. Afterwards, the temperature decreased to 200 °C and the catalyst was purged with He for 20 min to remove dissolved hydrogen in Ni. After that, the temperature decreased to 40 °C, at which the pulsed oxidation was performed using 2% O_2/He (prepared by mixing 10 mL/min of 10% O_2/He and 40 mL He). Stoichiometry of Ni/O_2 of 2 was used, corresponding to NiO formation. For surface concentration measurement a TCD (temperature conductivity detector) signal was used, while a mass spectrometer signal was used to confirm that no H_2O formation was observed, due to remaining H_2 after reduction. The cross-section area of the Ni atom of 0.065 nm^2 was assumed according to the literature [43]. We selected O_2 PSO based on comprehensive validation performed by Millet et al. [43]. In Table S2, the obtained values are presented, showing that the Ni-specific surface area is highest for the 10 wt% Ni/Al_2O_3 catalyst, followed by the commercial catalyst.

3.6. Development of the microkinetic model

The kinetic model will encompass the hydrogenation of three initial compounds, as depicted in Fig. 2, resulting in 12 potential compounds and 9 reactions. Given the similarity of the compounds, it is assumed that hydrogenation proceeds via a uniform mechanism for all. Each compound is represented by one of the possible structural isomers, although the compound may exist in another form or multiple forms.

This pertains to a three-phase system, wherein the solid catalyst is suspended within the liquid phase, while a hydrogen atmosphere envelops it. The quantity of dissolved hydrogen in the liquid phase correlates with the hydrogen pressure in the gas phase via Henry's constant.

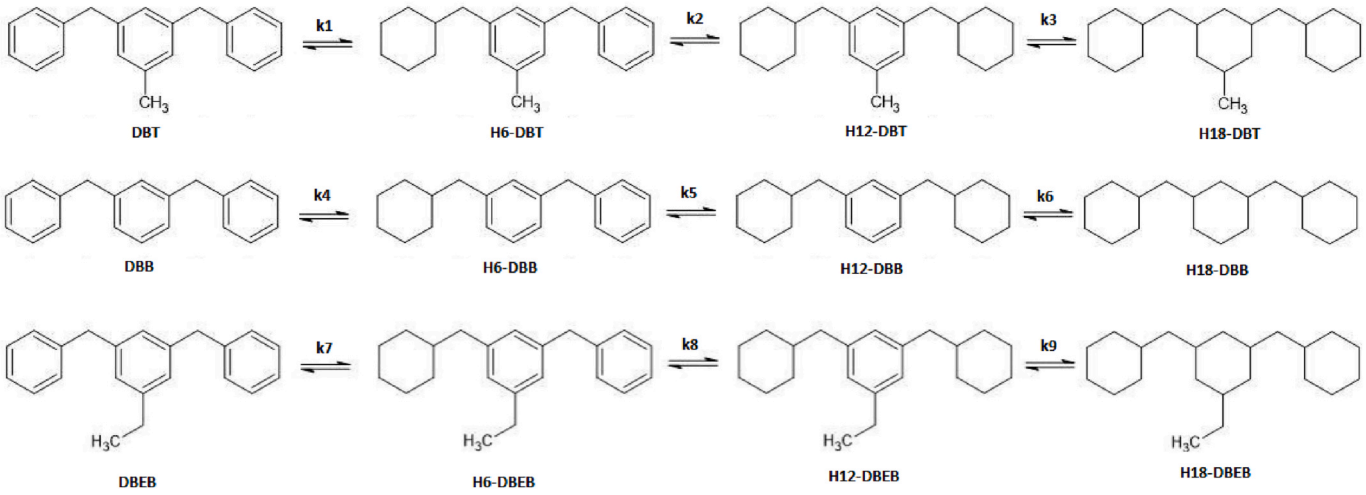

Fig. 2. Reaction scheme of DBT, DBB, and DBEB.

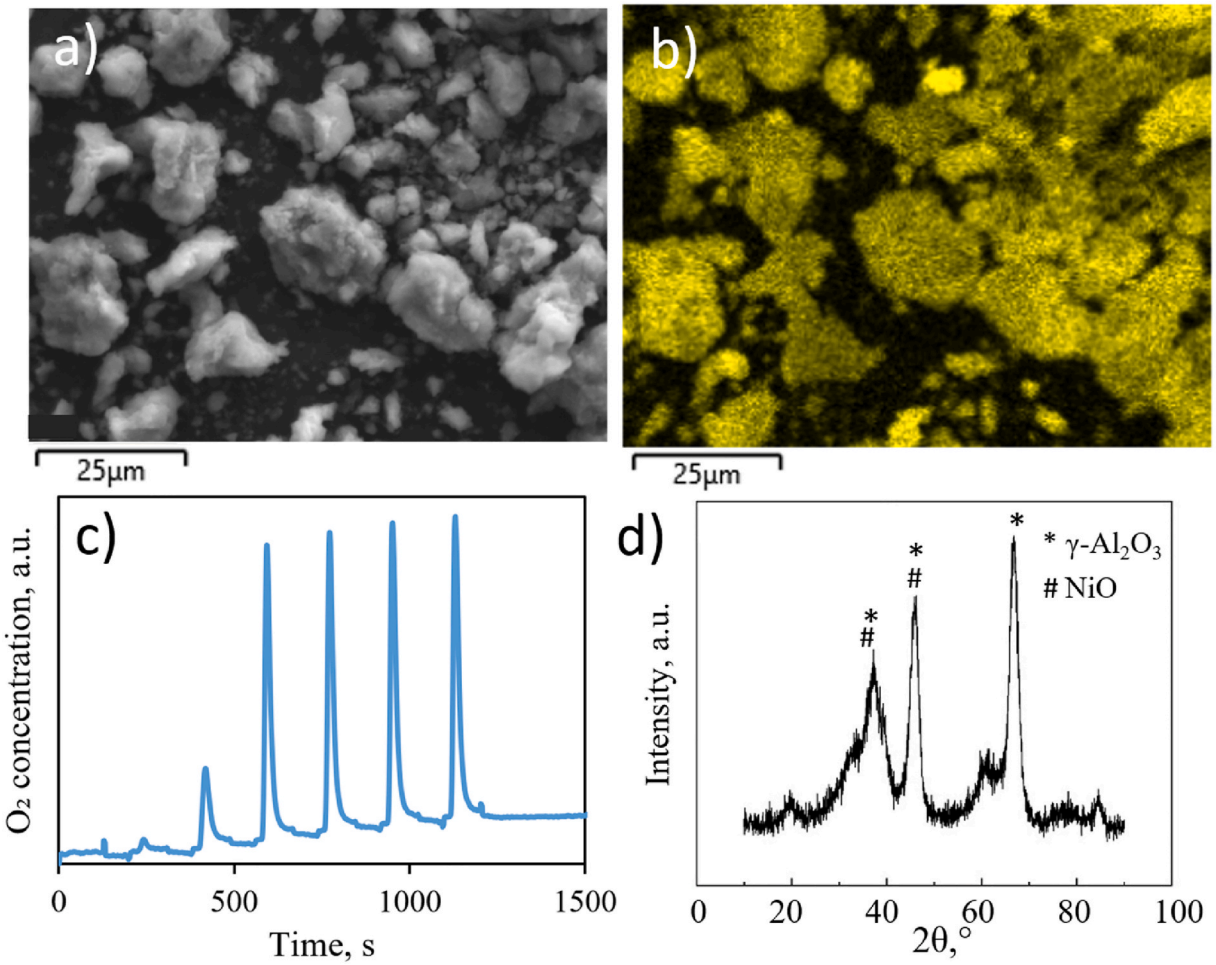

Fig. 3. SEM micrograph and b) EDS mapping showing uniform distribution of Ni (Ni Kα1) in synthesized 7% Ni/Al_2O_3 catalyst. c) example of O_2 pulsed surface oxidation of commercial 5% Ni/Al_2O_3, d) XRD of unreduced commercial catalyst.

The kinetic model will adhere to the Langmuir-Hinshelwood mechanism, under the following stipulations.

- The reaction transpires solely on the catalyst surface or within pores large enough to disregard mass transport limitations.
- In the scenario of a reaction without the catalyst (Fig. 4a), it is presumed that the initial compounds remain stable and do not decompose into alternative products.
- Considering no catalytic influence of supporting alumina (Fig. 4b). It is assumed that the reaction is confined to the metal surface, with

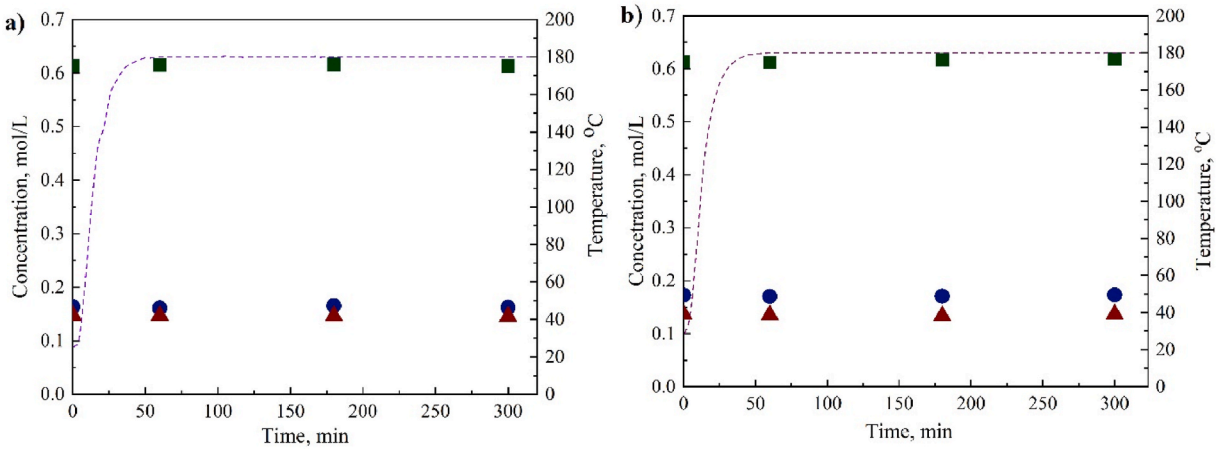

Fig. 4. The reaction of DBT, DBB, and DBEB a) without a catalyst and b) in the presence of γ-alumina (exposed to H_2 at 400 °C), where symbols represent experimental points and lines correspond to model values ■ DBT, ● DBB, ▲ DBEB, –temperature.

organic compounds and hydrogen solely adsorbing onto the metal surface.

- Vacant adsorption sites are considered uniform and independent of overall site coverage.
- Each site is occupied by either an organic or hydrogen molecule, as adsorption occurs competitively.
- Owing to high gas phase pressures (≥25 bar), the presence of other compounds in the gas phase is deemed negligible and hence disregarded in model resolution.
- Rates of adsorption and desorption of components surpass the rate of reaction on the catalyst surface, rendering it the rate-determining step.
- Rates of adsorption and desorption remain unaffected by temperature fluctuations.
- Reactions within the model are treated as irreversible due to the substantial concentration of hydrogen, which serves as a reactant.

The adsorption rate at the active site for an individual component (r_j^{ads}) depends on the adsorption constant (k_j^{ads}), the concentration of the component in the liquid phase (c_j^L), and the number of empty active sites (θ_{AM}) (Eq. (1)).

$$r_j^{ads} = k_j^{ads}\, c_j^L\, \theta_{AM} \tag{1}$$

The total number of active sites was obtained from Bjelić [44], where the same catalyst was measured using the temperature-programmed desorption method with carbon monoxide (CO-TPD), and the value is $3.7 \bullet 10^{-5}$ mol/g.

The desorption rate (r_j^{des}) depends only on the desorption constant (k_j^{des}) and the coverage of active sites with this component (θ_j) (Eq. (2)).

$$r_j^{des} = k_j^{des}\, \theta_j \tag{2}$$

The reaction rate on the catalyst surface (r_i^{surf}) depends on the coverage of active sites with the organic component (θ_j) and with hydrogen (θ_H) (Eq. (3)).

$$r_i^{surf} = k_i^{surf}\, \theta_j\, \theta_H \tag{3}$$

The kinetic model considers the reaction rate already during heating up to the final reaction temperature. The temperature and pressure in the reactor are recorded every 30 s in the program, allowing all constants dependent on these parameters to be precisely determined at any time in the model. For adsorption and desorption constants, it is assumed that they are independent of temperature since they do not represent the rate-limiting step. Reaction rate constants, as governed by the Arrhenius equation, are naturally temperature-dependent. T_1 represents the reference temperature, which is 453 K or 180 °C in this case, as most reactions occur at this temperature. T_2 is the actual temperature and the activation energy for a specific reaction (E_{ai}) (Eq. (4)).

$$k_i^{surf}(T_2) = k_i^{surf}(T_1) * exp\left(\frac{E_{a_i}}{R}\left(\frac{1}{T_1} - \frac{1}{T_2}\right)\right) \tag{4}$$

The concentration of dissolved hydrogen at the phase boundary (c_{H2}^{FM}) is related to the hydrogen pressure in the gas phase (p_{H2}) through Henry's law (Eq. (5)).

$$c_{H2}^{FM} = \frac{p_{H2}}{He} \tag{5}$$

whereas the Henry constant (He) is temperature-dependent, the data for this were obtained from Brunner [45], who described the phase equilibrium for hydrogen and hexane (Eq. (6)).

$$He = 640.9003 * \exp\left(-0.0041876 * T\right) \tag{6}$$

Although correlation was developed for the regime between 25 °C and 100 °C, we are utilizing it to assess H_2 solubility at higher temperatures, as one of model assumptions. To establish the equilibrium of components, it is necessary to ascertain the volumes of liquid (V_L) and gas (V_G) within the reactor. Additionally, for the equilibrium of hydrogen in the gas phase, the constant for mass transport (k_{GL} a) that was determined for this reactor system in the preceding section is required [46] (Eq. (7)).

$$\frac{dc_{H2}^G}{dt} = -k_{GL}a\left(c_{H2}^{FM} - c_{H2}^L\right)\frac{V_L}{V_G} \tag{7}$$

General equilibrium for the liquid phase with surface concentration of active sites (n_{TS}) (Eq. (8)):

$$\frac{dc_j^L}{dt} = -r_j^{ads} + r_j^{des}\frac{n_{TS}}{V_L} \tag{8}$$

Equilibrium for hydrogen in the liquid phase (Eq. (9)):

$$\frac{dc_{H2}^L}{dt} = +k_{GL}a\left(c_{H2}^{FM} - c_{H2}^L\right) - r_{H2}^{ads} + r_{H2}^{des}\frac{n_{TS}}{V_L} \tag{9}$$

General equilibrium for the coverage of active sites for a specific component, with the number of reactions I (Eq. (10)):

$$\frac{d\theta_j}{dt} = r_j^{ads}\frac{n_{TS}}{V_L} + r_j^{des} + \sum\nolimits_i^I \pm\, r_j^{surf} \tag{10}$$

Furthermore, the overall equilibrium for the coverage of all unoccupied active sites with a total of J components (Eq. (11)):

$$\frac{d\theta_{vs}}{dt} = \sum_j^J r_j^{ads}\frac{V_L}{n_{TS}} + \sum_j^J r_j^{des} + \sum_i^I \pm r_j^{surf} \quad (11)$$

This results in a set of ordinary differential equations that I solve using the Runge-Kutta (2,3) method with a selected MATLAB solver. The initial concentrations of all compounds are set to zero, except for DBT, DBB, and DBEB. Confidence intervals for the fitted parameters were determined using the confint function in MATLAB.Variables used are given in Table 2.

The degree of hydrogenation (DOH) was calculated based on the concentrations of hydrogenated species as (Eq. (12)):

$$DOH\ (\%) = \frac{(3\sum C_{H6} + 6\sum C_{H12} + 9\sum C_{H18})}{3\sum C_{LOCH,all}}\ x\ 100 \quad (12)$$

Hydrogen efficiency was calculated as (Eq. (13)):

$$DOH\ (\%) = \frac{(3\sum C_{H6} + 6\sum C_{H12} + 9\sum C_{H18})}{3\sum C_{LOCH,all}}\ x\ 100 \quad (13)$$

where Σc_{H6}, Σc_{H12}, and Σc_{H18} represent the summed concentrations of partially and fully hydrogenated species across all LOHC components (DBT, DBB, and DBEB), $\Sigma c_{LOCH,all)}$ is the total concentration of all species in the reaction mixture, and $\Sigma c_{LOHC,0}$ is the initial total concentration of hydrogen-lean LOHC species.

The DOH represents the extent of hydrogenation and reflects how far the reaction has progressed from the hydrogen-lean to hydrogen-rich state based on the distribution of intermediates and fully hydrogenated species. In contrast, hydrogen efficiency indicates how effectively the system utilises its theoretical hydrogen storage capacity, relating the amount of hydrogen incorporated into the LOHC to the maximum possible hydrogen uptake.

4. Results

4.1. Material characterization

The SEM investigation of the unreduced synthesized 7% Ni/Al_2O_3 catalyst (Fig. 3a and b) shows a generally uniform distribution of Ni over the Al_2O_3 particles, indicating successful material preparation. Additionally, SEM micrographs at low magnification (Supporting Fig. S3) reveal individual particles, confirming sizes below 100 μm and the absence of agglomeration. The XRD analysis of the unreduced commercial sample (Fig. 3d) indicates the presence of alumina in the γ-Al_2O_3 form (JCPDS 29-0063, [47]), while the presence of crystalline NiO (JCPDS 47-1049) cannot be easily dismissed due to the overlap between these two phases, however it is suggested that particles are either smaller than 4 nm or in an amorphous form. An adsorption isotherm graph is shown in Fig. S1. The shape of the isotherm and the presence of hysteresis indicate the presence of mesopores in the catalyst [48,49]. Additionally, further data was obtained using the method, as presented in Table S1. The specific surface area of the catalyst is notably high and considering the size of the DBT molecule and other compounds, it can be concluded that the contribution of micropores to the catalysis of the reaction is negligible.

The exposed surface Ni, determined by O_2 PSO (example for commercial catalyst in Fig. 3c, with the rest in Supporting Fig. S2), is summarised in Table 3. Based on Ni loading and specific surface area, the average Ni particle size was calculated to range between 21 nm and 42 nm for the synthesized catalyst, showing potential for improvement toward achieving even higher surface areas. Similar chemisorption-based Ni particle sizes (23 nm) were obtained by Afzal et al. [50] using 20% Ni/Al_2O_3 (Riogen), while numerical average transmission electron microscope Ni size was 8.4 nm, relating to significant particle size distribution of commercial material. However, when comparing the synthesized catalyst with the commercial one, we observed that we achieved significantly higher Ni dispersion (~35%) even at higher loading.

4.2. Results of model

No molecule H18-DBEB was detected in any of the reactions; therefore, it will not be displayed in the graphs. This reaction was also not considered in the development of the kinetic model. The reaction scheme for DBT is shown in green, DBB in blue, and DBEB in red (Fig. 4). All reactions presented so far have been utilized to construct the kinetic model. The kinetic data obtained from the model are summarised in Table 4. All constants fall within the same order of magnitude, a notable trend is observed where the activation energy decreases with the increasing number of hydrogenated rings in a given compound. This trend suggests that the first ring undergoes hydrogenation with the greatest difficulty, while subsequent rings are hydrogenated more easily. One possible explanation for this is that the benzene ring binds more strongly to the active site compared to the hydrogenated cyclohexane, due to its higher electron density and the presence of π-bonds. Since the compound contains three rings, the remaining two rings might be able to interact with adjacent active sites where hydrogen, necessary for hydrogenation, can bind. Once one or two rings in the compound are hydrogenated, the interaction strength with the active site is reduced.

For the hydrogenation of DBT, the range of activation energies is from 59.9 kJ/mol to 79 kJ/mol, while for DBB it ranges from 55.0 to 73.6 kJ/mol, indicating that DBB hydrogenates more quickly. To date, one kinetic study and analysis of Ni/Al_2O_3; the most common examples of kinetic models involve Ru catalysts. Li et al. [14] utilized a commercial 13 wt% Ni/Al_2O_3 catalyst, which demonstrated a superior yield compared to this study, with activation energies of 59.3, 56.1, and 64.6 kJ mol^{-1} for each reaction step. Kim et al. [24] calculated the activation energies for the first step of DBT hydrogenation (k_1) for the synthesized catalysts 0.5 wt% Ru/MgO and 0.5 wt% Ru/Al_2O_3, reporting values of 30.0 and 54.2 kJ/mol, respectively. The first two reactions were presented in Fig. 4 as an indicator of substrate reactivity. Standard conditions for conducting the reaction, against which other conditions are compared, include 180 °C, 75 bars of hydrogen, 100 mg of catalyst, a

Table 2
Definition of variables used in the microkinetic model.

Symbol	Description	Unit
c_j^L	Concentration of component j in liquid phase	$mol{\cdot}L^{-1}$
c_{H2}^L	Concentration of dissolved hydrogen	$mol{\cdot}L^{-1}$
c_{H2}^{FM}	Hydrogen concentration at phase boundary	$mol{\cdot}L^{-1}$
p_{H2}	Hydrogen pressure	bar
θ_j	Surface coverage of component j	–
θ_H	Surface coverage of hydrogen	–
θ_{VS}	Fraction of vacant active sites	–
r_j^{ads}	Adsorption rate	$mol{\cdot}L^{-1}{\cdot}s^{-1}$
r_j^{des}	Desorption rate	$mol{\cdot}L^{-1}{\cdot}s^{-1}$
r_i^{surf}	Surface reaction rate	$mol{\cdot}L^{-1}{\cdot}s^{-1}$
k_j^{ads}	Adsorption rate constant	$L{\cdot}mol^{-1}{\cdot}s^{-1}$
k_j^{des}	Desorption rate constant	s^{-1}
k_i^{surf}	Surface reaction rate constant	s^{-1}
$E_{a,i}$	Activation energy	$kJ{\cdot}mol^{-1}$
He	Henry's constant	$bar{\cdot}L{\cdot}mol^{-1}$
$k_{GL}a$	Gas–liquid mass transfer coefficient	s^{-1}
V_L	Liquid volume	L
V_G	Gas volume	L
n_{TS}	Total number of active sites	$mol{\cdot}g^{-1}$

Table 3
The Ni dispersion, Ni particle size and Ni specific surface area. The Ni dispersion and particle size were calculated based on nominal Ni loadings. 'com' denotes the commercial catalyst (Riogen).

Sample	D_{Ni}, %	S_{Ni}, m^2/g	c_{Ni}, μmol/g	$d_{Ni\text{-}O2\ PSO}$, nm
5 wt% Ni/Al_2O_3 com	3.6	1.2	31	28
5 wt% Ni/Al_2O_3	2.4	0.8	20	42
10 wt% Ni/Al_2O_3	4.9	3.3	84	21

Table 4
Kinetic parameters of hydrogenation reactions obtained of kinetic model.

i	Kinetic rate constant at 180 °C (k_i), min^{-1}	Activation energy (Ea_i), kJ/mol
1	61.8 ± 2.5	79.0 ± 3.9
2	57.8 ± 2.3	65.4 ± 2.8
3	36.1 ± 1.5	59.9 ± 2.5
4	60.5 ± 2.4	73.6 ± 3.8
5	103 ± 4.2	66.0 ± 2.6
6	33.1 ± 1.1	55.0 ± 2.1
7	87.7 ± 4.4	76.3 ± 3.8
8	43.7 ± 2.2	37.1 ± 1.9

DBT to hexane ratio of 10:30 (mL), and stirring at 800 rpm. The maximum reaction temperature was set at 220 °C, as this is close to the critical point of hexane at 234.5 °C. The maximum hydrogen pressure was 75 bar. In the reaction without a catalyst (a), no products were detected, and the initial concentration remained constant. This indicates that the substrate does not spontaneously react with hydrogen and is thermally stable, as previously mentioned. The subsequent reaction (b) took place in the presence of γ-alumina, reduced in the same manner as Ni/Al_2O_3 in later reactions. This demonstrates that the reaction does not occur on the support but only on the metallic active sites.

Subsequently, reactions were carried out with Ni/Al_2O_3 for use in the kinetic model. The parameters varied in these reactions included temperature, hydrogen pressure, substrate-to-solvent ratio, and catalyst amount. Since the initial concentrations of DBB and DBEB are significantly lower than the concentration of DBT and there are many compounds present in the system, the graphs are divided into two parts for better clarity.

4.3. Temperature effect

The figure illustrates the conversion rates at various temperatures where the reaction was conducted. Due to the notably low conversion achieved at 170 °C, it was deemed impractical to explore temperatures below this threshold. Although exploring temperatures above 220 °C could have been feasible, such an approach was avoided due to the proximity to the critical point of the system. From the data presented, it is evident that conversion rates increase substantially with rising temperatures. Notably, the conversion to full completion occurs most rapidly with DBB, which is the least sterically hindered molecule in the hydrogenation process. This is followed by DBT, with DBEB, the most sterically hindered molecule, reaching full conversion at the slowest rate. The observed trends highlight the significant impact of steric hindrance on the efficiency of hydrogenation reactions and underscore the importance of temperature control in optimizing conversion outcomes. When it comes to DBT, the conversion ranges from 43 mol% at 170 °C (Fig. 5a), 50 mol% at 180 °C and 190 °C (Fig. S5b and S5c) 70 mol% at 200 °C (Figs. 5b), 91 mol% at 210 °C (Fig. S5e) to complete conversion at the highest temperature of 220 °C (Fig. 5c). The concentration of 6H-DBT shows a trend that increases with temperature (Fig. 5), reaching a maximum at the highest temperature before starting to decrease (Fig. 5c), while the concentration of 12H-DBT continues to rise with selectivity from less than 1 mol% (Fig. 5a) to 50 mol % (Fig. 5c), and the concentration of 18H-DBT does not change significantly. In the case of DBB, complete conversion is achieved at a lower temperature of 210 °C (Fig. S5e). In Fig. S5e, experimental errors were determined. For DBT and hydrogenated products, the error was 2%; for DBEB, it was 6%; and for DBB, it was less than 1%, which is why it is not visible on the graph. The kinetic model that aligns with experimental results effectively describes the trends in concentration changes. It accurately reflects the deviations observed in the experimental data for DBT, 6H-DBT, 12H-DBT, and 16H-DBT. Notably, the most significant deviation occurs in the case of 6H-DBT (Fig. 5b), while the trends for all other intermediates are well captured by the model. Regarding the other compounds, DBB and DBEB, the largest deviation is noted in the case of 18H-DBB, whereas the trends for DBEB are consistently well represented by the model. For all reactions involving DBT, DBB, and DBEB, it is observed that the steps are temperature-dependent. In the case of DBT, the first two steps are highly dependent on temperature, whereas, for DBB and DBEB, all modeled steps are affected, as the concentration of 18H-DBEB was not detected in any of the experiments. Modisha et al. [51] used a 50 wt% Ni-based catalyst in the temperature range of 150-170 °C. The lower temperature, combined with a higher nickel content and a different type of reactor they used, a fixed-bed reactor, led to faster hydrogenation.

Nickel-based catalysts are highly active for DBT hydrogenation. Ali et al. [12] conducted a comparison of three different catalysts for H0-DBT hydrogenation, employing a stirred chemical reactor in a low-pressure system (0.9 MPa). The optimal temperature for hydrogenation was determined to be 170 °C, with catalytic activity ranking in the following order: Raney-Ni > 5 wt% Pd/Al_2O_3 > 5 wt% Ru/Al_2O_3 (Table 5, initial activity based on 2 h hydrogen capacity measurement). Furthermore Liu et al. investigated effect of different precious metals, and observed that (H_2-consumption based) TOF of Rh-based is even higher than of Ru-based material, although relative difference is smaller than between Ru and Raney-Ni. Overall, the mass-based activity and TOF of 10 wt% Ni/Al_2O_3 are the highest, comparing to the ones from the literature, although further in-house testing of Ru-based material would be needed to obtain completly consistent results.

4.4. Pressure effect

In the reactor system utilized in this study, all available hydrogen was introduced through pressurization at the start of the reaction. The initial hydrogen pressure used was 75 bar, with supplementary experiments conducted at 25 and 50 bar for model verification purposes. The influence of the initial hydrogen pressure of 75 bars is presented in Fig. 6. The initial pressure in the system controls the amount of the limiting reactant (hydrogen) involved in the LOHC hydrogenation. Consequently, it is expected that higher pressure values will substantially facilitate the hydrogenation process. When it comes to Fig. 6a, it is evident that lower pressure leads to minimal conversion, and at higher temperatures, this experiment was not repeated. Observing the profiles in Fig. 6a, b, and 6c, it can be seen that the difference in conversion is only noticeable between 25 and 50 bar for DBT, as well as for other LOHCs DBB and DBEB. In the case of the highest pressure of 75 bar, the concentration values of the intermediate are slightly higher. In all cases, neither 25, 50, nor 75 bars was sufficient for the complete hydrogenation of DBT to 18H-DBT.

When comparing different pressures (see Figs. 6 and 7), it is apparent that the conversion rate increases with rising pressure. Higher hydrogen gas pressure leads to a greater concentration of hydrogen in the liquid phase, which shifts the reaction equilibrium towards the products. This observation underscores the influence of pressure on enhancing reaction efficiency and shifting equilibrium in favour of product formation. When it comes to the higher temperature of 220 °C, we did not wish to experiment with the lowest pressure. There is a distinct difference between 50 and 75 bar at the higher temperature regarding DBT; in Fig. 7a and b, the conversion is significantly lower at higher pressure. In terms of selectivity for H6-DBT, the selectivity at higher pressure is twice as high, which is also the case for the intermediate H12-DBT. Regarding the desired product H18-DBT, its concentration was detected at higher pressure. For DBB, the conversion is higher, the concentration of all intermediates is greater, and it hydrogenates the fastest of all LOHCs due to the least steric hindrance. In the case of DBEB, it follows the same trend as the other two, with H12-DBEB also being detected in the secondary reaction. Higher pressure in combination with high temperature yields more favourable results; however, the reaction is slower than the reactions in the presence of Ru catalysts [36]. Regarding the model, it describes the concentration trends well at all pressures, indicating that the parameters are well defined, despite the presence of lower hydrogen concentrations in the system. In the literature, the effect of pressure

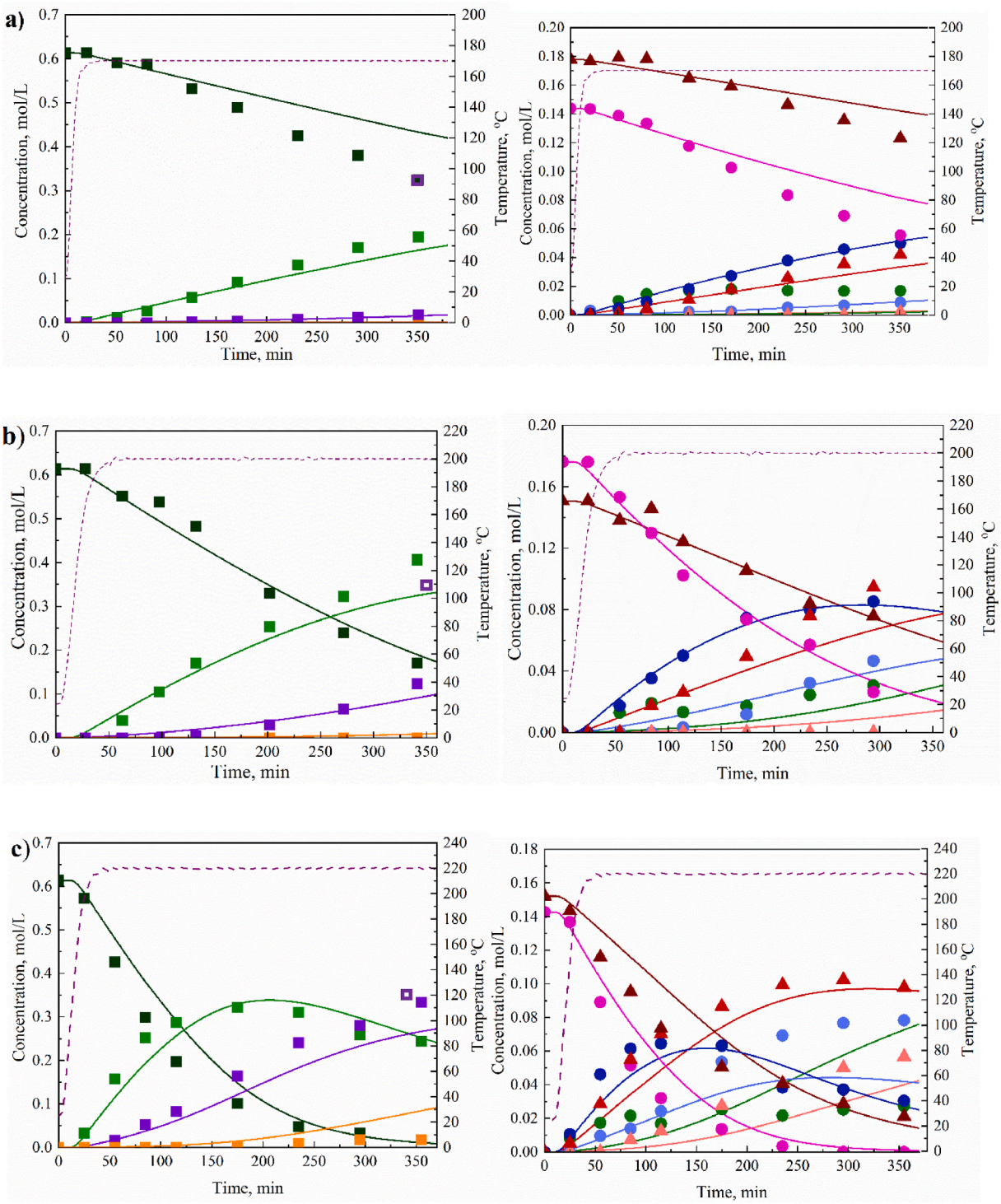

Fig. 5. *Effect of temperature on the reaction system at* 75 bar *hydrogen,* 100 mg *of catalyst, 10:*30 mL *ratio DBT in hexane ter 800 RPM mixing, with temperatures a) 170 °C, b) 200 °C and c) 220 °C, where symbols represent experimental points and lines correspond to model values.* ■ *DBT,* ■ *H6-DBT,* ■ *H12-DBT,* ■ *H18-DBT,* ● *DBB,* ● *H6-DBB,* ● *H12-DBB,* ● *H18-DBB,* ▲ *DBEB,* ▲ *H6-DBEB,* ▲ *H12-DBEB, – temperature,* □ *DBT exp. reference at 170 °C at the last time point.*

ranging from 2 to 6 MPa at 200 °C has been investigated, with higher pressures leading to faster hydrogenation of DBT [14]. Kim et al. [24] used 50 bars of hydrogen in their system, which was continuously maintained, proving to be an effective solution for this reaction.

4.5. Effect of DBT concentration

The variation in the DBT to hexane ratio results is shown in Fig. 8 (Fig. S6 more conditions). Increasing the ratio in favour of DBT leads to a decrease in conversion. Several factors may contribute to this

Table 5
Initial activity of H_2 consumption for DBT conversion comparison between various catalysts.

Catalyst	T, °C	P, bar	Activity, mmol H_2/(g •h)	D metal, %	TOF, min^{-1}	Ref.
10 wt% Ni/Al_2O_3	180	75	150	4.9	29.6	This study
5 wt% Ni/Al_2O_3 com	180	75	34.1	3.6	18.5	
5 wt%Rh/Al_2O_3	180	70	85.8	11.1	26.5	[20]
5 wt%Ru/Al_2O_3	180	70	73.1	11.4	21.6	
5 wt%Pd/Al_2O_3	180	70	1.5	10.9	0.5	
5 wt%Pt/Al_2O_3	180	70	12.6	12.4	6.6	
Raney-Ni	170	9	16.25	n.a.	n.a.	[12]
5 wt% Ru/Al_2O_3	170	9	10.75			
5 wt% Pd/Al_2O_3	170	9	6.75			
3 wt% Pd/C	170	9	5			

observation. It can be inferred that, even at lower ratios, all active sites may be optimally occupied, leading to potential issues with the adsorption of molecules onto these active sites. Additionally, the diffusion rate of DBT molecules decreases, and the viscosity of the liquid phase increases significantly, as DBT has a much higher viscosity compared to hexane. Generally at lower ratios, the conversion is higher. Further reduction in the concentration of DBT could shift the system from a reaction rate-limited regime to one where reactant adsorption becomes the limiting step. When it comes to higher concentrations of DBT and other LOHCs (Fig. 8c and d), a higher concentration leads to the excess reactants in the system not being able to undergo sufficient hydrogenation, as there is not enough hydrogen in the system, although at conversion reached DBT concentration decreases linearly with time pointing to the fact that H_2 pressure is almost constant. Regarding the model, despite the changed concentration of LOHCs in the system, it excellently describes the variation of all LOHC concentrations.

4.6. Effect of catalyst amount

With an increased amount of catalyst (see Fig. 9), the conversion rate is significantly higher, as more active sites are available for the reaction. A greater number of active sites results in higher concentrations visible in Fig. 9b under the same experimental conditions, with an increase in conversion in the system and higher yields. What we observe is that the concentration predicted by the model slightly differs from the actual concentration of the LOHCs. For DBT, the model predicts a lower conversion; regarding H6-DBT, the concentration peaks at 240 min and then begins to decline, while the model predicts a constant increase in concentration. In the case of H12-DBT, the experimentally measured concentration in the system is much higher than what the model describes. One solution to this discrepancy could involve considering and incorporating additional characteristics of the catalyst into the model, which would provide a better description of the system but would also make the model more complex.

Fig. 10 shows the execution of a reaction conducted for a longer duration than usual. The reaction was set up in the morning, as per standard procedure, and completed the following morning, running for nearly 23 h. By the end of the reaction, the pressure in the reactor had decreased significantly and remained relatively stable, indicating that the reaction had approached equilibrium.

The hydrogen pressure was not measured after cooling the reactor to room temperature. However, at 180 °C, the final pressure for this extended reaction was 18.5 bar, compared to 65.7 bar for reactions conducted for the usual duration. Although this extended reaction was not used for developing the model, the model for the reaction is shown. The model continues to perform well despite the extended reaction time.

4.7. Comparison of commercial and synthesized catalysts

The effect of nickel content in the catalyst was also investigated. Since this involves a different type of catalyst, laboratory-prepared catalysts were not included in the kinetic model.

Both commercial and laboratory-prepared 5 wt% Ni/Al_2O_3 catalysts yielded similar conversion rates (see Fig. S7a and S7b), indicating that the preparation method can be compared to industrial standards. As anticipated, the substrate conversion increases with a higher nickel content in the catalyst, as observed in cases Fig. S7c (7 wt% Ni) and Fig. 11 (10 wt% Ni).

An interesting comparison is made between Figs. 9b and 11. The former uses 200 mg of 5 wt% Ni/Al_2O_3, while the latter employs 100 mg of 10 wt% Ni/Al_2O_3, resulting in equal total nickel masses. The concentration of DBT at the end of the reaction drops to zero. The peak concentration of H6-DBT is reached later, at 300 min for the 10 wt% Ni/Al_2O_3 case, compared to the 5 wt% Ni/Al_2O_3, where the peak concentration is achieved earlier at 240 min. The concentration of H12-DBT is higher in the 5 wt% Ni/Al_2O_3 case. Lower concentrations of the active substance may be beneficial, as higher concentrations can lead to non-uniform distribution of active sites due to the tendency of the active substance to aggregate into larger particles during catalyst preparation. When we look at Table S3 in the supplementary file, we can see that the specific surface area is highest for the synthesized 10 wt% Ni/Al_2O_3, followed by the commercial 5 wt% Ni/Al_2O_3, and then the synthesized 5 wt% Ni/Al_2O_3. The synthesized 7 wt% Ni/Al_2O_3 was not included in the analysis, but the order of the specific surface area from highest to lowest matches the DBT conversion rates from highest to lowest. A recycling experiment, in which the catalyst was removed from the suspension, washed, reduced, and reused, was performed at 180 °C, 75 bar H_2, with 100 mg of catalyst and a 10 mL:30 mL DBT-to-hexane ratio at 800 rpm. The conversion of DBT decreased from 61% in the first cycle to 39% in the second cycle (conversion of DBB from 76% to 51%, conversion of DBEB from 38% to 15%), indicating partial catalyst deactivation, which may be attributed to Ni particle coarsening or carbon deposition [16]. This effect was not considered in the development of the kinetic model.

Additionally, experiments were conducted at a stirring speed of 400 rpm, as shown in Fig. S4, which yielded results similar to the standard reactions. This leads to the conclusion that there is no external mass transfer resistance. Although the literature reports stirring speeds of up to 1200 rpm [29], our chosen speed of 800 rpm ensures that the rate-limiting step is the surface reaction.

As shown in Fig. 4, no conversion of unsaturated compounds was achieved either homogeneously (or on the reactor walls) or by pure alumina. Therefore, a linear relationship between the number of surface Ni sites and the conversion rate of DBT is expected, especially since the average Ni particle size is greater than 20 nm in all cases, containing mainly plane and step surface sites (compared to edge and corner sites, which are more abundant at smaller particle sizes). By inspecting Fig. 12, we can see that this assumption generally holds, and a higher number of surface Ni sites leads to an increased conversion rate, validating the model assumption, although at smaller metal loading part of Ni could be hidden in micropores (<6% of Al_2O_3 support surface area represents micropores, Table S1), on which large DBT(-based) molecules could not react on. It could therefore be used as a proxy in the further development of the catalyst and in describing possible deactivation.

5. Discussion

The quantitative results of hydrogenation performance under different operating conditions are summarised in Table 6, enabling direct comparison of the effects of temperature, hydrogen pressure, catalyst loading, and LOHC-to-solvent ratio. A clear temperature

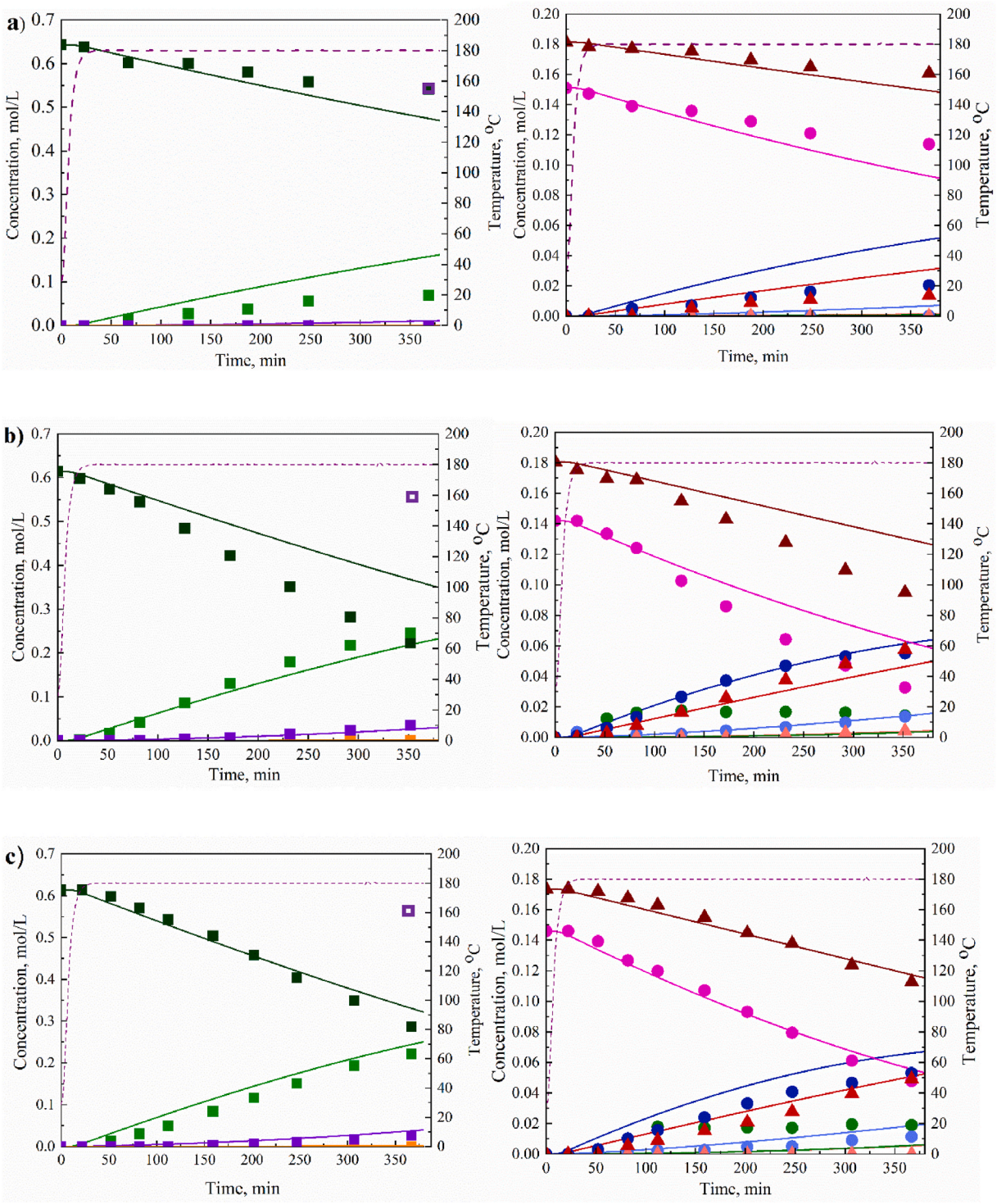

Fig. 6. Effect of pressure on the reaction system at 180 °C, with 100 mg catalyst, 10:30 mL ratio of DBT to hexane, and 800 RPM stirring, at hydrogen pressures of a) 25 bar, b) 50 bar, and c) 75 bar, where symbols represent experimental points and lines correspond to model values■ DBT, ■ H6-DBT, ■ H12-DBT, ■ H18-DBT, ●DBB, ●H6-DBB, ●H12-DBB, ●H18-DBB, ▲ DBEB, ▲ H6-DBEB, ▲ H12-DBEB, – temperature, □ DBT exp. reference at 25 bar at the last time point.

dependence is observed, with DOH increasing from 15.7% at 170 °C to 52.1% at 220 °C, indicating kinetically controlled behaviour. Higher temperatures promote the formation of more saturated species, leading to improved hydrogen uptake and utilisation. Hydrogen pressure has a pronounced effect on system performance. At 180 °C, reducing the pressure from 75 bar to 25 bar leads to a drastic drop in DOH (from ~20 to 27% to 3.7%), confirming that hydrogen availability is a limiting factor under low-pressure conditions. This suggests that both hydrogen solubility and transport to the catalyst surface are critical.The LOHC-to-solvent ratio also influences performance, as deviations from the

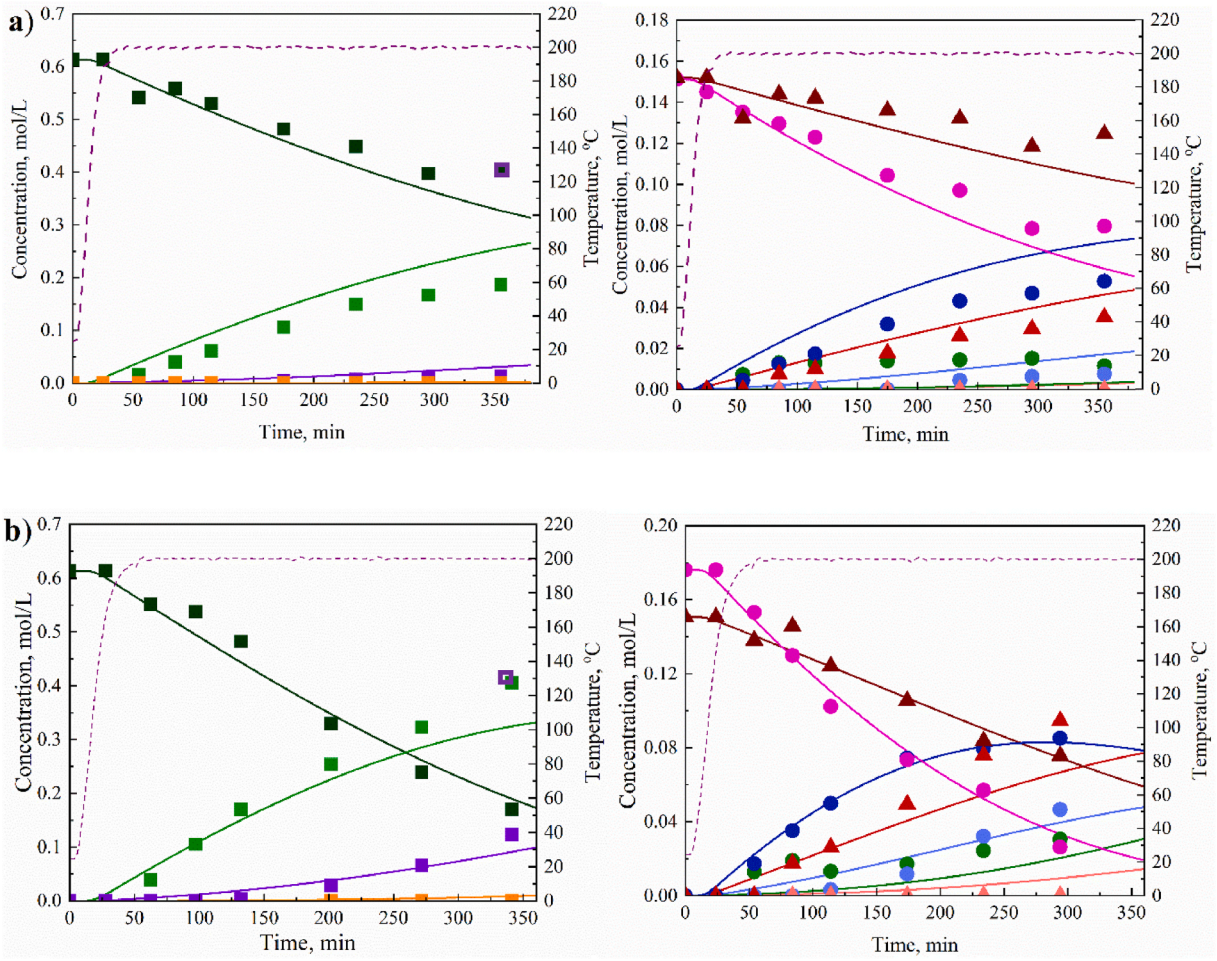

Fig. 7. Effect of pressure on the reaction system at 200 °C, with 100 mg catalyst, 10:30 mL ratio of DBT to hexane, and 800 RPM stirring, at hydrogen pressures of a) 50 bar, and b) 75 bar, where symbols represent experimental points and lines correspond to model values■ DBT, ■ H6-DBT, ■ H12-DBT, ■ H18-DBT, ●DBB, ●H6-DBB, ●H12-DBB, ●H18-DBB, ▲ DBEB, ▲ H6-DBEB, ▲ H12-DBEB, – temperature, ▣ DBT exp. reference at 50 bar at the last time point.

standard 10:30 composition result in variations in DOH, indicating the role of dilution and mass transfer effects. Catalyst loading affects hydrogenation behaviour as well. Increasing the catalyst amount from 0.1 g to 0.2 g leads to a notable increase in DOH (from 27.6% to 47.2%), highlighting the importance of active site availability. The influence of catalyst composition was further evaluated for samples synthesized with different Ni loadings (5–10 wt%, Experiments 14–16). Slight variations in DOH (18.4–44.8%) and hydrogen efficiency (19.9–36.3%) suggest that higher Ni content improves catalytic activity, although the effect is less pronounced than that of temperature or pressure. The small difference between DOH and hydrogen efficiency across all experiments indicates efficient utilisation of hydrogen, with minimal losses.

Overall, hydrogenation performance is governed by a combined effect of kinetics and hydrogen availability, where temperature controls the reaction rate and pressure determines hydrogen accessibility.

The quality of the model fit was evaluated using the coefficient of determination (R^2), with values summarised in Table S2. An overall R^2 value of 0.98645 indicates excellent agreement between experimental and modeled data. High agreement was also observed for individual systems, with R^2 values of 0.99028 for DBT, 0.96365 for DBB, and 0.95715 for DBEB. The slightly lower R^2 value observed for DBEB is attributed to its lower concentration levels compared to the main species. Since the model parameters were estimated using a least-squares objective function, deviations at low concentration levels can have a more pronounced effect on the fitting quality. This suggests that the model captures the dominant reaction pathways, while minor deviations are primarily associated with low-concentration species. Linear regression analyses used for the determination of R^2 values are provided in Fig. S8a–d in the Supplementary Information.

The obtained kinetic parameters are in good agreement with literature data reported for DBT hydrogenation systems. Reported activation energies for Ni-based catalysts are typically in the range of 56–65 kJ/mol [14], while noble metal catalysts such as Ru/Al_2O_3 exhibit similar values of 56–67 kJ/mol [20]. This indicates that the activation barriers obtained in the present study fall within the expected range, confirming the physical relevance of the proposed kinetic model.

6. Conclusion, implications and future work

The hydrogenation of DBT was investigated using a nickel-based catalyst, offering a more cost-effective alternative to the commonly used noble metal systems. A kinetic model was developed and successfully applied to describe the experimental data over a wide range of conditions. Although the achieved DBT conversion was relatively modest, the results clearly indicate that there is significant room for improvement. In particular, higher temperatures (potentially through

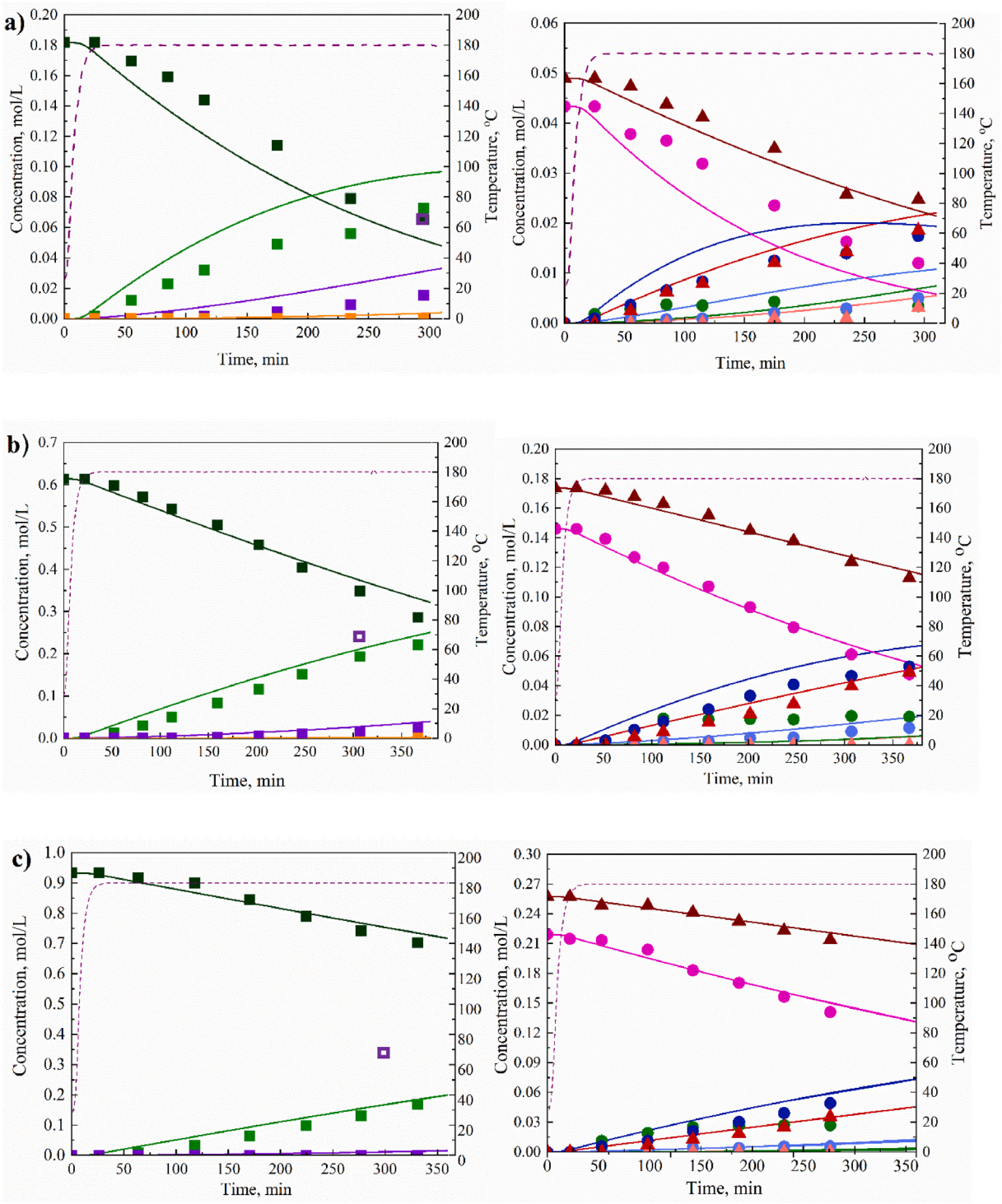

Fig. 8. Effect of the DBT to hexane ratio on the reaction system at 180 °C, 75 bar hydrogen pressure, 100 mg catalyst, and 800 RPM stirring, with ratios of a) 2.5:37.5 mL, b) 10:30 mL, and c) 15:25 mL, where symbols represent experimental points and lines correspond to model values ■ DBT, ■ H6-DBT, ■ H12-DBT, ■ H18-DBT, ●DBB, ●H6-DBB, ●H12-DBB, ●H18-DBB, ▲ DBEB, ▲ H6-DBEB, ▲ H12-DBEB, – temperature, □ DBT exp. relative reference at ratio 2.5:37.5 mL at the last time point.

solvent modification or removal), optimisation of the DBT ratio, and increased catalyst loading could all contribute to enhanced performance. Additionally, operating at higher and more stable hydrogen pressures would likely accelerate the reaction and could enable much higher conversions, even when using nickel-based catalysts.

The developed model provides a reliable representation of the system, showing that a relatively simple kinetic approach can still capture the key reaction trends. The estimated activation energies are in good agreement with literature values, despite the limited number of studies focusing on nickel in this context. Overall, these findings highlight the

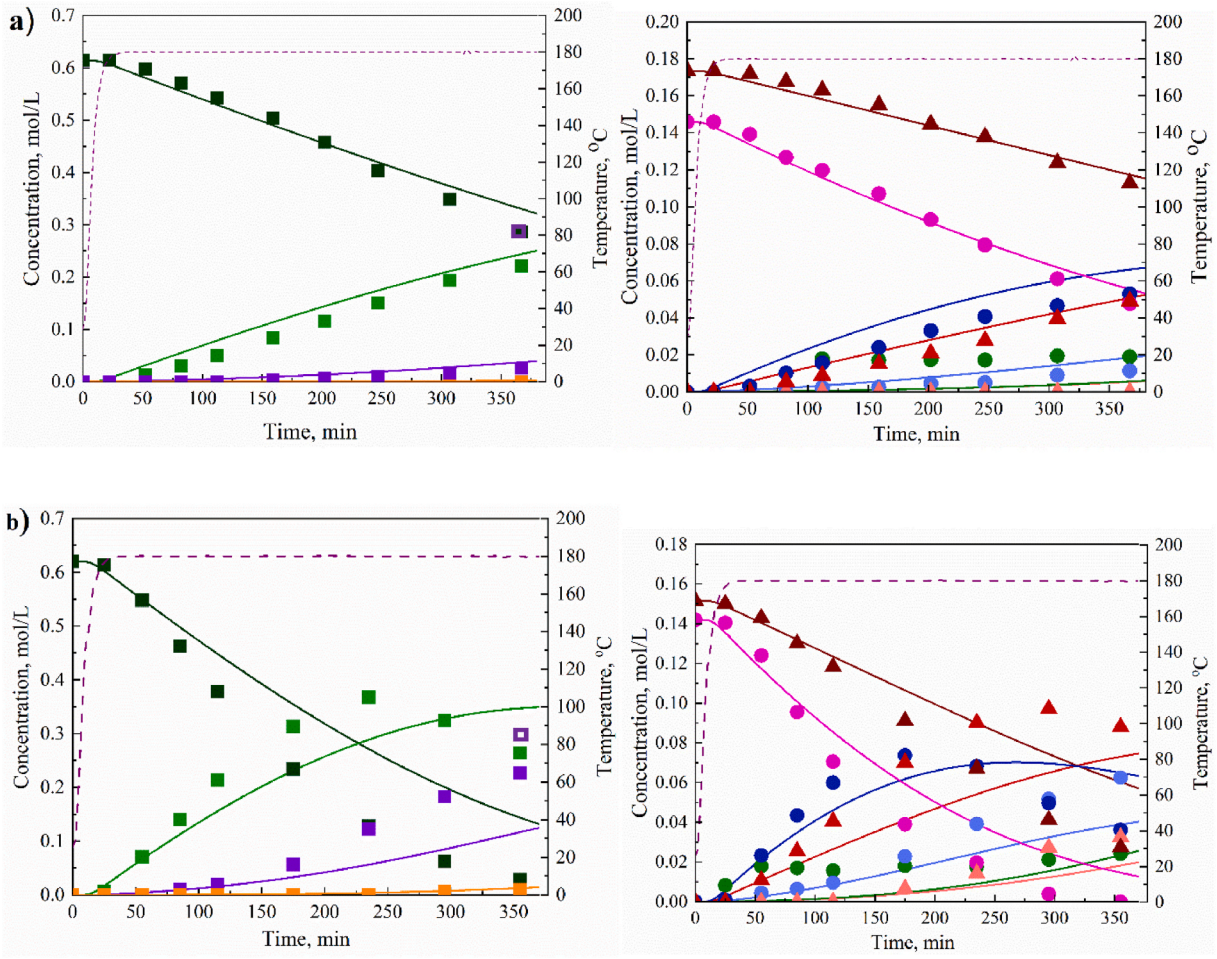

Fig. 9. *Effect of catalyst amount on the reaction system at 180 °C,* 75 bar *hydrogen pressure, 10:*30 mL *ratio of DBT to hexane, and 800 RPM stirring, with catalyst masses of a)* 100 mg *and b)* 200 mg*, where symbols represent experimental points and lines correspond to model values.* ■ *DBT,* ■ *H6-DBT,* ■ *H12-DBT,* ■ *H18-DBT,* ● *DBB,* ● *H6-DBB,* ● *H12-DBB,* ● *H18-DBB,* ▲ *DBEB,* ▲ *H6-DBEB,* ▲ *H12-DBEB,* – *temperature,* □ *DBT exp. reference with* 100 mg *of catalyst at the last time point.*

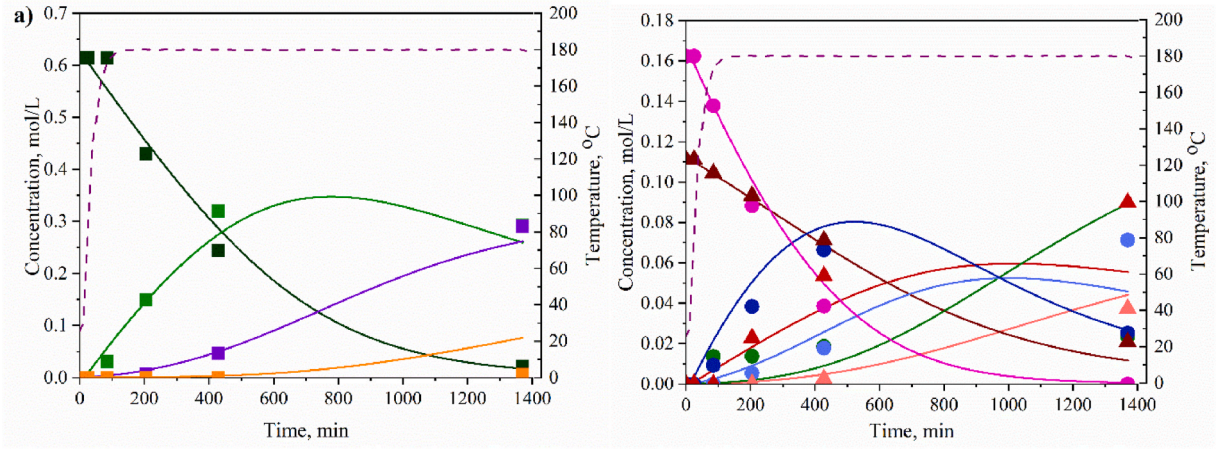

Fig. 10. Overnight reaction at 180 °C, 75 bar hydrogen pressure, 10:30 mL Ratio of DBT to hexane, 100 mg Catalyst, and 800 RPM Stirring, where symbols represent experimental points and lines correspond to model values. ■ DBT, ■ H6-DBT, ■ H12-DBT, ■ H18-DBT, ● DBB, ● H6-DBB, ● H12-DBB, ● H18-DBB, ▲ DBEB, ▲ H6-DBEB, ▲ H12-DBEB, – temperature.

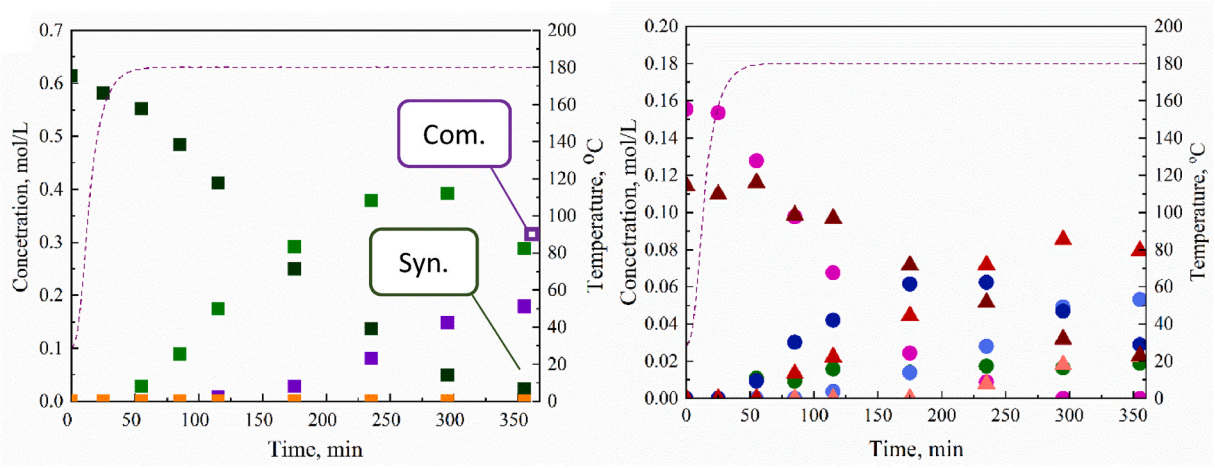

Fig. 11. Comparison of commercial (5 wt% Ni/Al_2O_3) and synthesized catalysts (10 wt% Ni/Al_2O_3) at 180 °C, 75 bar hydrogen pressure, 10:30 mL ratio of DBT to hexane, and 800 RPM stirring. All catalyst masses are 100 mg. Symbols represent experimental points and lines correspond to model values. ■ DBT, ■ H6-DBT, ■ H12-DBT, ■ H18-DBT, ●DBB, ●H6-DBB, ●H12-DBB, ●H18-DBB, ▲ DBEB, ▲ H6-DBEB, ▲ H12-DBEB, – temperature, ▣ DBT exp. reference with commerical 5 wt% Ni/Al_2O_3 at the last time point.

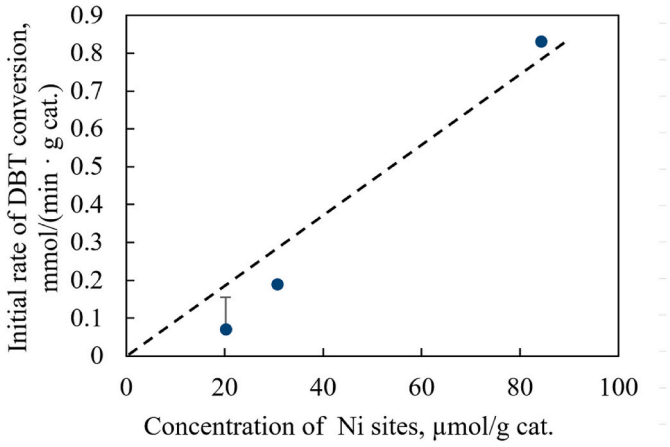

Fig. 12. Correlation between number of surface Ni sites, determined using O_2 PSO and the rate of DBT conversion.

potential of nickel-based catalysts as a practical and economically attractive option, while also pointing towards the need for further optimisation of catalyst composition and operating conditions to achieve higher conversion levels.

In addition to the presented results, the developed microkinetic model provides insight into the behaviour of multi-component LOHC systems under a wide range of operating conditions, which is directly relevant for process optimisation and reactor design. The ability of the model to describe multiple components (DBT, DBB, and DBEB) and their corresponding hydrogenation pathways highlights its applicability beyond simplified single-compound systems.

At the same time, the obtained results also indicate that further considerations are required for practical implementation. In particular, the sensitivity of reaction rates to operating conditions suggests that mass and heat transfer effects may become increasingly important at larger scales. In addition, long-term catalyst performance remains a key factor for reliable operation under industrial conditions. These findings demonstrate that, while the proposed approach provides a robust kinetic framework, its full potential can be realised through integration with reactor-scale models and process-level optimisation, supporting its relevance for industrial LOHC applications.

Table 6
Summary of hydrogenation performance under different operating conditions at the end of the reaction.

Exp	T (°C)	P (bar)	Catalyst (g)	DOH (%)	H_2 efficiency (%)	LOCH:HEX ratio [ml]
1	170	75	0.1	15.7	14.6	10:30
2	180	75	0.1	21.7	18.0	10:30
3	180	50	0.1	18.3	16.2	10:30
4	180	25	0.1	3.7	3.5	10:30
5	210	75	0.1	39.2	29.7	10:30
6	180	75	0.1	8.6	8.2	15:25
7	200	75	0.1	32.0	36.1	10:30
8	190	75	0.1	22.1	22.6	10:30
9	180	75	0.1	27.6	24.0	05:35
10	180	75	0.2	47.2	41.3	10:30
11	200	25	0.1	12.8	12.8	10:30
12	200	50	0.1	38.7	30.7	10:30
13	180	75	0.1	21.7	18.0	10:30
14[a]	180	75	0.1	18.4	19.9	10:30
15[b]	180	75	0.1	22.1	22.8	10:30
16[c]	180	75	0.1	44.8	36.3	10:30
17	200	50	0.1	22.3	24.6	10:30
18	220	75	0.1	52.1	53.0	10:30
19	180	75	0.1	23.2	20.1	2.5:37.5

[a] -5%wt Ni/Al_2O_3 synthesized.
[b] -7%wt Ni/Al_2O_3 synthesized.
[c] - 10% Ni/Al_2O_3 synthesized.

CRediT authorship contribution statement

Emilija Rakić Krstić: Writing – review & editing, Writing – original draft, Methodology, Investigation, Funding acquisition, Formal analysis, Data curation. **Filip Bergelj:** Writing – original draft, Methodology, Funding acquisition, Formal analysis, Data curation. **Anže Prašnikar:** Writing – review & editing, Writing – original draft, Methodology, Funding acquisition, Formal analysis, Data curation. **Brett Pomeroy:** Writing – original draft, Methodology, Investigation, Funding acquisition, Formal analysis, Data curation. **Blaž Likozar:** Writing – review & editing, Visualization, Validation, Supervision, Resources, Project administration, Conceptualization.

Declaration of competing interest

The authors declare that they have no known competing financial interests or personal relationships that could have appeared to influence the work reported in this paper.

Acknowledgments

The authors would like to appreciatively acknowledge the financial support of the Slovenian Research Agency (Program P2-0152 and research project N2-0316). HyBReED cofounded by: European Union: NextGenerationEU, Republic of Slovenia, Slovenian Research Agency (ARIS) and Slovenian Ministry of Higher Education, Science and Innovation

Appendix A. Supplementary data

Supplementary data to this article can be found online at https://doi.org/10.1016/j.ijhydene.2026.155320.

References

[1] Niermann M, Timmerberg S, Drünert S, Kaltschmitt M. Liquid organic hydrogen carriers and alternatives for international transport of renewable hydrogen. Renew Sustain Energy Rev 2021;135. https://doi.org/10.1016/j.rser.2020.110171.
[2] Niermann M, Beckendorff A, Kaltschmitt M, Bonhoff K. Liquid organic hydrogen carrier (LOHC) – assessment based on chemical and economic properties. Int J Hydrogen Energy 2019;44:6631–54. https://doi.org/10.1016/j.ijhydene.2019.01.199.
[3] Kim A, Yoo Y, Kim S, Lim H. Comprehensive analysis of overall H2 supply for different H2 carriers from overseas production to inland distribution with respect to economic, environmental, and technological aspects. Renew Energy 2021;177:422–32. https://doi.org/10.1016/j.renene.2021.05.127.
[4] Asif F, Hamayun MH, Hussain M, Hussain A, Maafa IM, Park YK. Performance analysis of the perhydro-dibenzyl-toluene dehydrogenation System—A simulation study. Sustain Times 2021;13. https://doi.org/10.3390/su13116490.
[5] Shi L, Qi S, Qu J, Che T, Yi C, Yang B. Integration of hydrogenation and dehydrogenation based on dibenzyltoluene as liquid organic hydrogen energy carrier. Int J Hydrogen Energy 2019:5345–54. https://doi.org/10.1016/j.ijhydene.2018.09.083.
[6] Meng J, Zhou F, Ma H, Yuan X, Wang Y, Zhang J. A review of catalysts for methylcyclohexane dehydrogenation. Top Catal 2021;64:509–20. https://doi.org/10.1007/s11244-021-01465-6.
[7] Rao PC, Yoon M. Potential liquid-organic hydrogen carrier (Lohc) systems: a review on recent progress. Energies 2020;13. https://doi.org/10.3390/en13226040.
[8] Liu J, Chen X, Xu J, Zhu S, Cheng H, Yang G, Han X, Zhang L, Li Y, Han S. A new strategy for enhancing the cycling stability of superlattice hydrogen storage alloys. Chem Eng J 2021;418:129395. https://doi.org/10.1016/j.cej.2021.129395.
[9] Rakić E, Grilc M, Likozar B. Liquid organic hydrogen carrier hydrogenation–dehydrogenation: from ab initio catalysis to reaction micro-kinetics modelling. Chem Eng J 2023;472. https://doi.org/10.1016/j.cej.2023.144836.
[10] Modisha PM, Ouma CNM, Garidzirai R, Wasserscheid P, Bessarabov D. The prospect of hydrogen storage using liquid organic hydrogen carriers. Energy Fuels 2019;33:2778–96. https://doi.org/10.1021/acs.energyfuels.9b00296.
[11] Shi L, Zhou Y, Qi S, Smith KJ, Tan X, Yan J, Yi C. Pt catalysts supported on H2and O2Plasma-Treated Al2O3for hydrogenation and dehydrogenation of the liquid organic hydrogen carrier pair dibenzyltoluene and perhydrodibenzyltoluene. ACS Catal 2020;10:10661–71. https://doi.org/10.1021/acscatal.0c03091.
[12] Ali A, Kumar GU, Lee HJ. Investigation of hydrogenation of Dibenzyltoluene as liquid organic hydrogen carrier. In: Mater. Today proc. Elsevier Ltd; 2021. p. 1123–7. https://doi.org/10.1016/j.matpr.2020.03.232.
[13] Park S, Abdullah MM, Seong K, Lee S. Kinetic analysis of dibenzyltoluene hydrogenation on commercial Ru/Al2O3 catalyst for liquid organic hydrogen carrier. Chem Eng J 2023;474:145743. https://doi.org/10.1016/j.cej.2023.145743.
[14] Li J, Zhang Q, Zhang J, Gao R, Zhang X, Zou JJ, Pan L. Intrinsic kinetics of dibenzyltoluene hydrogenation over a supported Ni catalyst for green hydrogen storage. Ind Eng Chem Res 2024;63:220–32. https://doi.org/10.1021/acs.iecr.3c03613.
[15] Müller K, Aslam R, Fischer A, Stark K, Wasserscheid P, Arlt W. Experimental assessment of the degree of hydrogen loading for the dibenzyl toluene based LOHC system. Int J Hydrogen Energy 2016;41:22097–103. https://doi.org/10.1016/j.ijhydene.2016.09.196.
[16] Sisáková K, Podrojková N, Oriňaková R, Oriňak A. Novel catalysts for dibenzyltoluene as a potential liquid organic hydrogen carrier use-A mini-review. Energy Fuels 2021;35:7608–23. https://doi.org/10.1021/acs.energyfuels.1c00692.
[17] Aakko-Saksa PT, Cook C, Kiviaho J, Repo T. Liquid organic hydrogen carriers for transportation and storing of renewable energy – review and discussion. J Power Sources 2018;396:803–23. https://doi.org/10.1016/j.jpowsour.2018.04.011.
[18] Jeong K, Yook H, Lee SH, Han HJ, Jung Y, Han S, Shin SY, Choi M, Kwon S, Lee JH, Kim SJ, Kim SM, Han JW, Park JH. Benzyl-methylbenzyl-benzene: improving hydrogen storage and release performance of dibenzyltoluene based liquid organic hydrogen carrier. Chem Eng J 2024;488:150927. https://doi.org/10.1016/j.cej.2024.150927.
[19] Sekine Y, Higo T. Recent trends on the dehydrogenation catalysis of Liquid organic hydrogen carrier (LOHC): a review. Top Catal 2021;64:470–80. https://doi.org/10.1007/s11244-021-01452-x.
[20] Liu L, Zhu T, Xia M, Zhu Y, Ke H, Yang M, Cheng H, Dong Y. Identifying noble metal catalysts for the hydrogenation and dehydrogenation of dibenzyltoluene: a combined theoretical-experimental study. Inorg Chem 2023;62:17390–400. https://doi.org/10.1021/acs.inorgchem.3c02721.
[21] Lei N, Qiu S, Zhang L, Zhao G, Wang S, Liu K. Synergistic effect between Pt and CrOx on reversible hydrogenation and dehydrogenation of dibenzyltoluene. Ind Eng Chem Res 2025;64:4761–70. https://doi.org/10.1021/acs.iecr.4c03878.
[22] Shirvani S, Hartmann D, Smith KJ. ScienceDirect two-dimensional Mo 2 C : an efficient promoter for hydrogen storage and release from a liquid organic hydrogen carrier. Int J Hydrogen Energy 2023;48:12309–20. https://doi.org/10.1016/j.ijhydene.2022.11.291.
[23] Ali A, Rohini AK, Noh YS, Moon DJ, Lee HJ. Hydrogenation of dibenzyltoluene and the catalytic performance of Pt/Al2O3 with various Pt loadings for hydrogen production from perhydro-dibenzyltoluene. Int J Energy Res 2022;46:6672–88. https://doi.org/10.1002/er.7604.
[24] Kim TW, Kim M, Kim SK, Choi YN, Jung M, Oh H, Suh YW. Remarkably fast low-temperature hydrogen storage into aromatic benzyltoluenes over MgO-supported Ru nanoparticles with homolytic and heterolytic H2 adsorption. Appl Catal B Environ 2021;286. https://doi.org/10.1016/j.apcatb.2021.119889.
[25] Jorschick H, Preuster P, Dürr S, Seidel A, Müller K, Bösmann A, Wasserscheid P. Hydrogen storage using a hot pressure swing reactor. Energy Environ Sci 2017;10:1652–9. https://doi.org/10.1039/c7ee00476a.
[26] Yoo JK, Lee SH, Park TI, Lee JH, Lee KY. Unraveling the impact of Niobia promotion on Pt/Al2O3 for enhanced catalytic performance in benzyltoluene reactions. ACS Catal 2025;15:114–28. https://doi.org/10.1021/acscatal.4c03543.
[27] Shi L, Zhou Y, Tan X, Qi S, Smith KJ, Yi C, Yang B. The effects of alumina morphology and Pt electron property on reversible hydrogenation and dehydrogenation of dibenzyltoluene as a liquid organic hydrogen carrier. Int J Hydrogen Energy 2022;47:4704–15. https://doi.org/10.1016/j.ijhydene.2021.11.076.
[28] Auer F, Hupfer A, Bösmann A, Szesni N, Wasserscheidpeter P. Influence of the nanoparticle size on hydrogen release and side product formation in liquid organic hydrogen carrier systems with supported platinum catalysts. Catal Sci Technol 2020;10:6669–78. https://doi.org/10.1039/d0cy01173h.
[29] Do G, Preuster P, Aslam R, Bösmann A, Müller K, Arlt W, Wasserscheid P. Hydrogenation of the liquid organic hydrogen carrier compound dibenzyltoluene-reaction pathway determination by 1H NMR spectroscopy. React Chem Eng 2016;1:313–20. https://doi.org/10.1039/c5re00080g.
[30] Jorschick H, Bulgarin A, Alletsee L, Preuster P, Bösmann A, Wasserscheid P. Charging a liquid organic hydrogen carrier with wet hydrogen from electrolysis. ACS Sustainable Chem Eng 2019;7:4186–94. https://doi.org/10.1021/acssuschemeng.8b05778.
[31] Kim TW, Park S, Oh J, Shin CH, Suh YW. Hydrogenation of the LOHC compound monobenzyl toluene over ZrO2-supported Ru nanoparticles: a consequence of Zirconium hydroxide's surface hydroxyl group and surface area. ChemCatChem 2018;10:3406–10. https://doi.org/10.1002/cctc.201800565.
[32] Jorschick H, Vogl M, Preuster P, Bösmann A, Wasserscheid P. Hydrogenation of liquid organic hydrogen carrier systems using multicomponent gas mixtures. Int J Hydrogen Energy 2019;44:31172–82. https://doi.org/10.1016/j.ijhydene.2019.10.018.
[33] Ruiz JR, García-Mancha N, Campana R, Tardío C. Catalytic role of nickel in hydrogen storage and release using dibenzyltoluene as a liquid organic hydrogen carrier. Energies 2025;18. https://doi.org/10.3390/en18164429.
[34] Jeong H, Kim TW, Kim M, Han GB, Jeong B, Suh YW. Mesoporous acidic SiO2-Al2O3Support boosts nickel hydrogenation catalysis for H2Storage in aromatic LOHC compounds. ACS Sustainable Chem Eng 2022;10:15550–63. https://doi.org/10.1021/acssuschemeng.2c04978.
[35] Li J, Zhang J, Zhang S, Gao R, Zhang X, Pan L, Zou JJ. Intrinsic kinetics of benzyltoluene hydrogenation over a supported Ni catalyst for green hydrogen storage. Int J Hydrogen Energy 2024;49:1586–96. https://doi.org/10.1016/j.ijhydene.2023.10.216.
[36] Tomić A, Pomeroy B, Todić B, Likozar B, Nikačević N. Catalytic hydrogenation reaction micro-kinetic model for dibenzyltoluene as liquid organic hydrogen carrier. Appl Energy 2024;365. https://doi.org/10.1016/j.apenergy.2024.123262.
[37] D'Ambra F, Faucheux V, Nicolas E, Cantat T, Gébel G, Hajiyev P. Direct enthalpy measurement for hydrogenation of liquid organic hydrogen carriers by differential scanning calorimetry under H2 pressure. Ind Eng Chem Res 2024;63:13157–68. https://doi.org/10.1021/acs.iecr.4c01739.
[38] Huynh ND, Hur SH, Kang SG. Tuning the dehydrogenation performance of dibenzyl toluene as liquid organic hydrogen carriers. Int J Hydrogen Energy 2021;46:34788–96. https://doi.org/10.1016/j.ijhydene.2021.08.039.
[39] Jorschick H, Geißelbrecht M, Eßl M, Preuster P, Bösmann A, Wasserscheid P. Benzyltoluene/dibenzyltoluene-based mixtures as suitable liquid organic hydrogen carrier systems for low temperature applications. Int J Hydrogen Energy 2020;45:14897–906. https://doi.org/10.1016/j.ijhydene.2020.03.210.

[40] Hydrogenious LOHC technologies GmbH, how LOHC works. https://hydrogenious.net/how/. [Accessed 13 April 2026].
[41] M.O.H.C. (LOHC) – A. based on chemical and economic properties Niermann, Beckendorff A, Kaltschmitt M, Bonhoff K. Liquid organic hydrogen carrier (LOHC) – assessment based on chemical and economic properties. Int J Hydrogen Energy 2019;44:6631–54. https://doi.org/10.1016/j.ijhydene.2019.01.199.
[42] Ba J, Gao R, Shi D, Nessa HA, Shi C, Zhang X, Pan L, Zou JJ. Progress in catalysts for hydrogen storage/release in MBT/DBT based LOHCs: a review. Chem Commun 2025;61:8619–31. https://doi.org/10.1039/d5cc01352f.
[43] Millet MM, Frei E, Algara-Siller G, Schlögl R, Tarasov A. Surface titration of supported Ni catalysts by O2-pulse thermal analysis. Appl Catal Gen 2018;566:155–63. https://doi.org/10.1016/j.apcata.2018.08.023.
[44] Bjelić A, Grilc M, Likozar B. Bifunctional metallic-acidic mechanisms of hydrodeoxygenation of eugenol as lignin model compound over supported Cu, Ni, Pd, Pt, Rh and Ru catalyst materials. Chem Eng J 2020;394:124914. https://doi.org/10.1016/j.cej.2020.124914.
[45] Brunner E. Solubility of hydrogen in 10 organic solvents at 298.15, 323.15, and 373.15 K. J Chem Eng Data 1985:269–73.
[46] Grilc M, Likozar B. Levulinic acid hydrodeoxygenation, decarboxylation and oligmerization over NiMo/Al2O3 catalyst to bio-based value-added chemicals: modelling of mass transfer, thermodynamics and micro-kinetics. Chem Eng J 2017;330:383–97. https://doi.org/10.1016/j.cej.2017.07.145.
[47] Hosseini SA, Niaei A, Salari D. Production of γ-Al_2O_3 from Kaolin. Open J Phys Chem 2011;1:23–7. https://doi.org/10.4236/ojpc.2011.12004.
[48] Ambroz F, Macdonald TJ, Martis V, Parkin IP. Evaluation of the BET theory for the characterization of meso and microporous MOFs. Small Methods 2018;2:1–17. https://doi.org/10.1002/smtd.201800173.
[49] Rahman MM, Muttakin M, Pal A, Shafiullah AZ, Saha BB. A statistical approach to determine optimal models for IUPAC-classified adsorption isotherms. Energies 2019;12. https://doi.org/10.3390/en12234565.
[50] Afzal S, Prakash AV, Littlewood P, Marks TJ, Weitz E, Stair PC, Elbashir NO. Controlling the rate of change of Ni dispersion in commercial catalyst by ALD overcoat during dry reforming of methane. Int J Hydrogen Energy 2020;45:12835–48. https://doi.org/10.1016/j.ijhydene.2020.03.008.
[51] Modisha P, Bessarabov D. Stress tolerance assessment of dibenzyltoluene-based liquid organic hydrogen carriers. Sustain Energy Fuels 2020;4:4662–70. https://doi.org/10.1039/d0se00625d.